PL-TR-91-3009

Final Report
for the period
February 1989 to
July 1990

TWENTY FIRST CENTURY PROPULSION CONCEPT

May 1991

Author:
R.L. Talley

Veritay Technology, Inc.
4845 Millersport Highway
East Amherst NY 14051

F04611-89-C-0023

Approved for Public Release

Distribution is unlimited. The OL-AC PL Technical Services Office has reviewed this report and it is releaseable to the National Technical Information Service, where it will be available to the general public, including foreign nationals.

Prepared for the: **Phillips Laboratory**

Air Force Systems Command
Propulsion Directorate
Edwards AFB CA 93523-5000

NOTICE

When U. S. Government drawings, specifications, or other data are used for any purpose other than a definitely related Government procurement operation, the fact that the Government may have formulated, furnished, or in any way supplied the said drawings, specifications, or other data, is not to be regarded by implication or otherwise, or in any way licensing the holder or any other person or corporation, or conveying any rights or permission to manufacture, use or sell any patented invention that may be related thereto.

FOREWORD

This final report was submitted by Veritay Technology, Inc., East Amherst NY, on completion of Small Business Inovation Research (SBIR) Contract F04611-89-C-0023 with the OL-AC Phillips Laboratory (AFSC), Edwards AFB CA. PL Project Manager was Dr. Frank Mead.

This report has been reviewed and is approved for release and distribution in accordance with the distribution statement on the cover and on the DD Form 1473.

Franklin B. Mead Jr.

FRANKLIN B. MEAD, JR.
Project Manager

Stephen L. Rodgers

STEPHEN L. RODGERS
Chief, Emerging Technologies Branch

FOR THE COMMANDER

David W. Lewis

DAVID W. LEWIS, MAJOR, USAF
Acting Director
Fundamental Technologies Division

REPORT DOCUMENTATION PAGE

Form Approved
OMB No. 0704-0188

1. AGENCY USE ONLY (Leave blank)	2. REPORT DATE	3. REPORT TYPE AND DATES COVERED
	May 1991	Final report from 7 Feb 89-7 Jul 90

4. TITLE AND SUBTITLE
TWENTY FIRST CENTURY PROPULSION CONCEPT (U)

5. FUNDING NUMBERS
PE 65502F
PR 3058
TA 0026
C F04611-89-C-0023

WUIS 345247

6. AUTHOR(S)
Robert L. Talley

7. PERFORMING ORGANIZATION NAME(S) AND ADDRESS(ES)
Veritay Technology, Inc.
4845 Millersport Highway
P.O. Box 305 (7V715)
East Amherst NY 14051

8. PERFORMING ORGANIZATION REPORT NUMBER
F06-9-1

9. SPONSORING/MONITORING AGENCY NAME(S) AND ADDRESS(ES)
Phillips Laboratory
Propulsion Directorate
Air Force Systems Command
Edwards Air Force Base CA 93523-5000

10. SPONSORING/MONITORING AGENCY REPORT NUMBER
PL-TR-91-3009

11. SUPPLEMENTARY NOTES Project Manager was Dr Franklin S. Mead, Jr., OLAC PL/RKFT, Edwards AFB CA 93523-5000. The Propulsion Directorate formerly known as the Astronautics Laboratory (AFSC).
COSATI CODES: 22/01; 21/03; 09/03

12a. DISTRIBUTION/AVAILABILITY STATEMENT
APPROVED FOR PUBLIC RELEASE; DISTRIBUTION IS UNLIMITED

12b. DISTRIBUTION CODE

13. ABSTRACT *(Maximum 200 words)*

This Phase II SBIR contract was concerned with exploring the Biefield-Brown effect which allegedly converts electrostatic energy directly into a propulsive force in a vacuum environment.

Activities under this program emphasized the experimental exploration of this electrostatic thrust-generation concept to confirm or deny its existence, to verify its operation under high vacuum conditions, and to establish an experimental database via tests with candidate devices to permit the nature and magnitude of its thrust to be determined.

To meet these goals an improved laboratory test configuration was developed for quantifying the electrostatically induced propulsive forces on selected environmental devices. This configuration utilized a vacuum chamber and diffusion pump arrangement which extended conditions to the 1 microtorr range. While attempts were made to increase the driving DC voltage to 50 kV or more, the driving voltages were generally limited to about 19 kV to avoid electrical breakdown problems. Boundary effects arising from the presence of induced surface charges on the walls of the vacuum chamber surrounding the test devices were significant, and had to be taken into account in using the torsion pendulum system to make thrust force measurements.

Direct experimental results of this investigation indicate that no detectable pro-

14. SUBJECT TERMS	15. NUMBER OF PAGES
Biefield-Brown Effect; Electrostatic Field Propulsion; Electrostatic Force Generation; Advanced Propulsion Techniques; Torsion Pendulum Force Measurements	16. PRICE CODE

17. SECURITY CLASSIFICATION OF REPORT	18. SECURITY CLASSIFICATION OF THIS PAGE	19. SECURITY CLASSIFICATION OF ABSTRACT	20. LIMITATION OF ABSTRACT
UNCLASSIFIED	UNCLASSIFIED	UNCLASSIFIED	UNLIMITED

PL-TR-91-3009

Block 13 (continued)

pulsive force was electrostatically induced by applying a static potential difference up to 19 kV between the electrodes of test devices under conditions in which electrical breakdowns did not occur.

Near the conclusion of this program, force generation effects were examined using a high dielectric constant, ceramic piezoelectric material between electrodes of an asymmetric test device under voltage conditions which caused repetitive electrical breakdowns to occur. Very limited test results of this type suggest that anomalous forces were produced, and these may warrant further consideration in the future.

Table of Contents

List of Figures

List of Figures (cont)

List of Tables

INTRODUCTION

The objective of this study was to experimentally investigate the Biefield-Brown effect, which allegedly converts electrostatic energy directly into a propulsive force in a vacuum environment.

In the 1920s, Dr. Paul Biefield and Townsend T. Brown discovered that a propulsive force was generated when a large DC electrical potential difference is applied between shaped electrodes fixed and separated from one another by a dielectric member. Under these conditions a net force results which acts on the entire electrode/dielectric body and typically causes it to move in the direction of the positive electrode.

This concept may represent a direct field-field, or field-vacuum interaction scheme with the potential for producing thrust without the conventional action-reaction type of momentum transfer brought about by ejective expenditure of an on-board fuel. The significance of this field propulsion concept to launching and/or maneuvering payloads in space is potentially very great.

This concept has received cursory attention over many years since its discovery, but at the outset of the present effort it was still inadequately explored and remained without confirmed operation in a vacuum, without quantitative characterization, and without an adequate theoretical basis for its operation.

This force generation technique was explored briefly under a Phase I Small Business Innovative Research (SBIR) program using a laboratory test configuration consisting of a vacuum chamber and a torsion fiber type measurement system. This system permitted the direct assessment of electrostatically induced propulsion forces on selected experimental devices. Initial tests were

conducted at atmospheric pressure and over the vacuum range down to 10 millitorr, using an applied DC voltage. Preliminary results of these tests were interpreted as being supportive of the Biefield-Brown effect. However, these initial results were inconclusive because inadequate vacuum conditions were achieved; correspondingly, the applied voltage was limited to 1.5 kV or less.

In the follow-on Phase II SBIR effort reported here the goals were two fold. The first was to improve selected features of the test hardware, extend the vacuum conditions to 1 microtorr and increase the driving DC voltage to 50 kV or more. The second was to establish an experimental data base via tests with candidate devices to permit the nature and quantitative characteristics of this electrostatically induced propulsive force to be determined. It was expected that tests conducted at the extremes noted should confirm or deny the existence of a real propulsive force under these conditions.

Activities under this program emphasized improving the experimental test configuration and conducting tests to develop a data base. The overall experimental effort still centered on making direct measurements of electrostatically induced propulsive forces on candidate test devices, inasmuch as details of the nature of the Brown effect were too sketchy to provide a reliable base for interpreting indirect measurements.

This report discusses the various features of the investigation, including the experimental configuration and instrumentation, the efforts to deal with severe electrostatic boundary effects, test techniques and results, observed anomalies, and overall conclusions.

The experimental results of this investigation indicate that no detectable propulsive force was electrostatically induced by

applying a static potential difference up to 19 kV between device electrodes, either with or without a spatial divergence of the electric field and energy density within that field. The minimum detectable force in these experiments was about 2×10^{-9} N. Under these test conditions, no detectable electrical breakdowns occurred.

Near the very end of this program, a few brief attempts were made to examine the force generation effects with pulsed fields, at 19 kV which was just under breakdown conditions. Some of these results, noted under observed anomalies, may warrant further consideration in the future.

EXPERIMENTAL CONFIGURATION

Background

During the Phase I SBIR program, we designed and fabricated a laboratory test configuration for directly quantifying Biefield-Brown type electrostatically induced propulsive forces on selected experimental devices. The configuration, discussed in detail in References 1 and 2, used a cylindrical vacuum chamber oriented with its axis vertical, together with a single torsion-fiber-type measurement system for direct assessment of propulsive forces. Geometrical and electrical symmetries were incorporated into the test set-up and in the device designs. These were to minimize the influence of electrostatically induced reaction forces which might arise from nearby bodies, including the walls of the vacuum chamber itself.

This arrangement permitted tests to be conducted either at atmospheric pressure or over a range of partial vacuum conditions. Investigation of the Brown effect over a range of subatmospheric conditions was considered desirable, since

electrical wind effects are known to be significant under normal atmospheric conditions, and can be responsible for some of the results often attributed to the Brown effect. Force measures taken over a range of vacuum levels would allow extrapolation of results to vacuum levels below about 100 microtorr (the expected lower limit of vacuum for the initial test set-up) where effects of electric wind should be negligible.

The initial experimental configuration was found to have several shortcomings that are briefly noted here for information. These have served as guidance in improving the test set-up for the Phase II program. These features include the following:

- Frictionless electrical contacts (consisting of platinum points touching liquid mercury) were used to feed the high voltage electrical power to the test devices while a force measurement was being made. The points and test devices were mounted on a figure-eight type device holder and were suspended by a single torsion fiber. The depth of penetration of the contact points into the mercury was critical to achieve nearly frictionless performance. While this depth could be adjusted to the nearest 0.001 in from outside the chamber by raising or lowering the vacuum-sealed rod holding the torsion fiber, it was difficult to achieve test-to-test reproducibility of this depth setting. In turn, the reproducibility of measured forces may have suffered.

- The electrical insulation used on the high voltage feed-through into the vacuum chamber needed to be of higher quality to help preclude voltage breakdown across the insulation surfaces.

- Improved quality of electrical insulation was also needed in the device holder for separating the device electrodes, to permit operation at higher voltages and to avoid unwanted electrical breakdowns.

- Operation at a better vacuum, say below about 100 microtorr, was needed to achieve vacuum breakdown potentials in excess of a few tens of kilovolts. Such high vacuum was also needed to improve the breakdown characteristics experienced with the electrical insulators noted previously.

- Operation in this better vacuum regime was also desirable to assure that residual ion or electrical wind effects were not influencing the electrostatically induced forces under examination.

- Within the proposed vacuum regime, the liquid mercury would no longer be suitable for use as part of the frictionless electrical contacts. At room temperature, mercury boils at a pressure of about 500 microtorr.

- The Brown and Sharpe No. 34 tinned copper wire, used as a single torsion fiber in the force measuring system, often showed a small drift in the system zero point setting. A better fiber choice was a conducting tungsten fiber, but such a fiber was not available for use in the Phase I program.

In Reference 2, an analysis of the torsion pendulum was conducted to show that the force measuring approach selected can be employed either in a static or in a dynamic mode.

In the static mode, the test devices suspended by the torsion fiber are assumed to be initially at rest. Upon

application of a steady propulsive force, the fiber twists until its restoring torque balances the applied torque. The propulsive force can then be found from the observed twist, using the fiber torsional calibration value and the moment arms of the applied force.

In the dynamic mode, the test devices suspended by a torsion fiber are allowed to swing free and to undergo small angular oscillations about the vertical fiber axis. This system behaves as a linear torsion pendulum. This oscillatory behavior results from propulsive, boundary, or random torques acting against the restoring torque of the fiber, and the oscillations are typically damped by the frictional forces. If the pendulum is shielded so the random torques are negligible (such as in a grounded, metallic, vacuum chamber), the pendulum motion can be analyzed in terms of the propulsive, boundary, and frictional forces, and can be used in a general way to characterize the nature of simple forms of propulsive forces. In particular, a steady propulsive force can be applied to the oscillating pendulum and the resulting angular offset of the mid point (or average position) of the pendulum swing from the initial zero position is directly proportional to the force, as in the static mode above. Mainly, this mode of force application was used in the current program, although the use of force pulses applied over single half cycles were explored experimentally in Reference 2.

Test Configuration and Subsystems

A block diagram of the overall test layout used in this Phase II investigation is given in Figure 1. This layout incorporates features to minimize the influence of shortcomings noted in the previous section. This figure shows schematically the key components, their grouping into functional subsystems, and their interconnections within the subsystems.

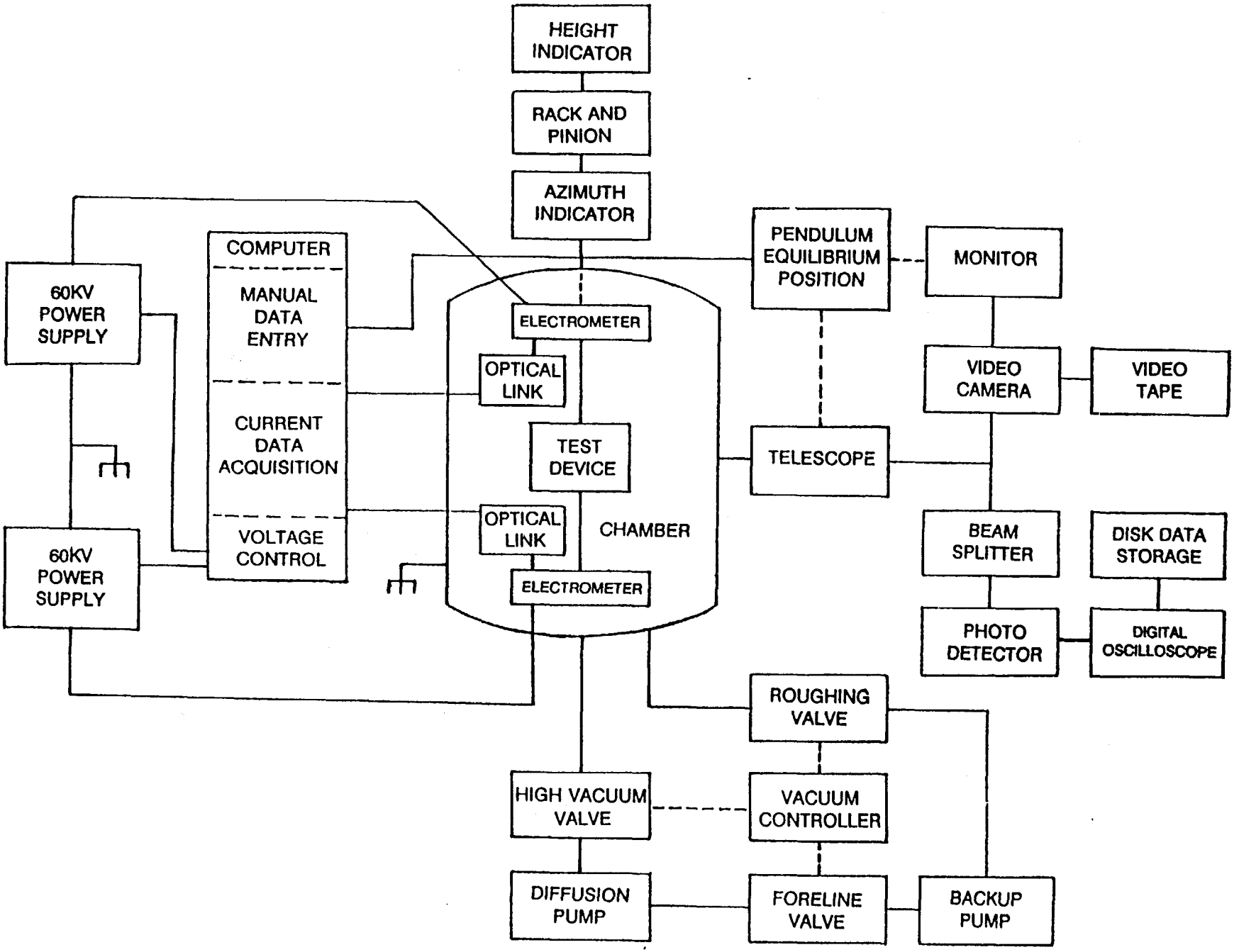

Figure 1. Block Diagram of Overall Test Layout

The subsystems include the following:

1. Main test configuration, which encompasses the vacuum chamber and the components within its interior.

2. Torsion fiber subsystem, which is the central element for measuring propulsive forces, is located inside the chamber.

3. Optical readout and data acquisition subsystem, used for extracting and recording torsion fiber twist information, which is directly related to applied torques and, hence, forces.

4. Electrical subsystem, which includes the high voltage sources (each with feedback control), the data acquisition subsystem for current, and an XT computer for control of power supplies and the electrometer-transceivers.

5. Vacuum subsystem, which includes a roughing pump, diffusion pump, ionization gauge, valve controller, and accessories related to achieving and quantifying partial vacuum conditions in the chamber.

6. Test devices, which are essential to the meaningful exploration of the Brown effect.

Main Test Configuration

The main test configuration, including the torsion fiber subsystem, is shown schematically in Figure 2. The central feature of this arrangement was the AISI type 316 stainless steel vacuum chamber. It was approximately 1.04 m (40.8 in) in diameter by 1.52 m (60 in) overall height with a

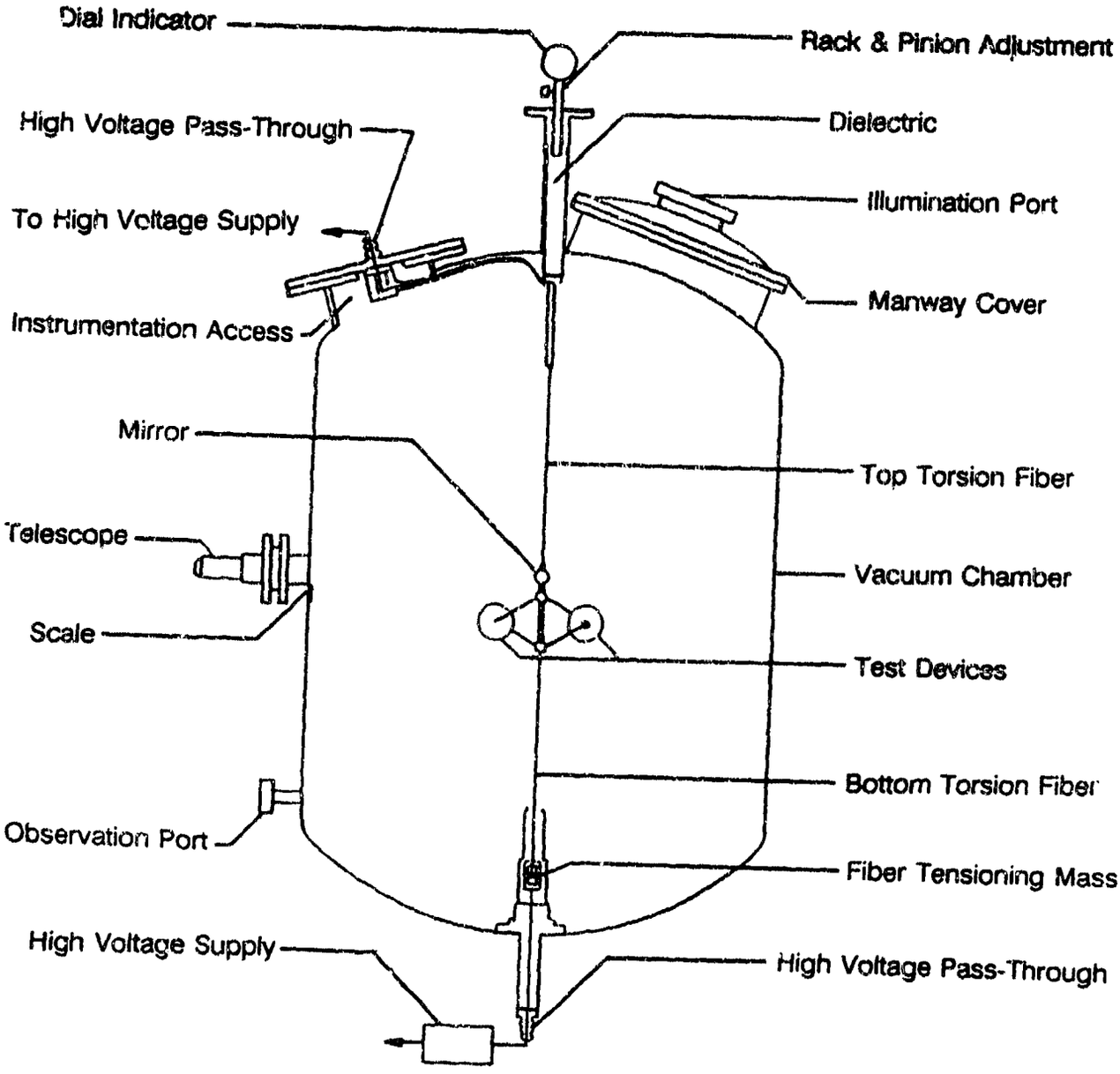

Figure 2. Test Configuration Schematic

1.17 m (46 in) straight side and a welded, dished top and bottom. Access to the chamber was provided through a 0.51 m (20 in) top manway. Smaller ports were also available and were used as instrumentation and illumination ports. A 0.20 m (8 in) port (not shown), offset from the chamber axis, was cut in the bottom of the chamber. A surface flange was welded in place adjacent to this port for close-up mounting of the diffusion pump. The chamber was mounted on legs (not shown) with leveling screws for adjustment of the vertical axis of the chamber.

Candidate propulsion test devices were mounted in tandem on an improved, insulated figure-eight type device support. To overcome the earlier problems encountered with the use of mercury as frictionless electrical contacts, here a pair of tungsten torsion fibers was used to feed high voltage electricity to the test devices. One fiber was suspended from the top of the chamber down to the test device support. A second fiber passed from this support to a special mass--electrical contact arrangement near the bottom of the chamber. The latter tensioned the lower fiber and effectively produced a constant-tension, taut torsion fiber system.

The electrical inputs to the test devices were fed from two high voltage DC power supplies through low-loss, high voltage pass-through fittings into the chamber. One pass-through was in an off-center top port of the chamber; the other was in the center bottom port. Cabling from the upper fitting connected to the upper tungsten taut fiber through an electrically floating (battery driven) electrometer. A similar electrical feed arrangement was used for the lower tungsten fiber.

The conducting fibers, in turn, supplied high voltage to the test devices via conducting arms of the device support structure.

A force measurement consisted of determining the average angular twist of the taut torsion fiber system caused by action of the force. This, together with the fiber calibration constant and moment arms of the test devices, permitted the force on the devices to be evaluated. The average angular twist of the torsion fibers was measured using a telescope, mirrors mounted to the test device support, and scales fastened to the chamber wall.

Torsion Fiber Subsystem

The measurement of forces generated by electrostatically driven test devices was carried out using a dual, taut torsion fiber subsystem. The test devices together with their support structure were suspended by the upper fiber, and this unit operated as a torsion pendulum in a dynamic mode. Accordingly, the devices and holder were free to undergo small angular oscillations about the vertical fiber axis with respect to an angular equilibrium position. The torque to twist the fibers was provided by the device or boundary generated force components directed perpendicular to both the fiber axis and to radial moment arms. These arms are defined by the fiber axis and the central lines of force through the test devices.

Two such test devices were directed in tandem and mounted on the figure-eight support structure shown in Figure 3, at "equal" radial distances from the fiber axis. This revised device support structure incorporated features of better electrical isolation of component parts, better symmetry to minimize asymmetric forces which are not test device related, and reduced use of dielectric components to just a single central element. The single element shown was a fire-polished 5.0 mm glass rod, coaxial with the fiber used to join the identical top and bottom aluminum conductor tubes of the support arms. The average moment arm distances for tests conducted in this program were 0.09778 m.

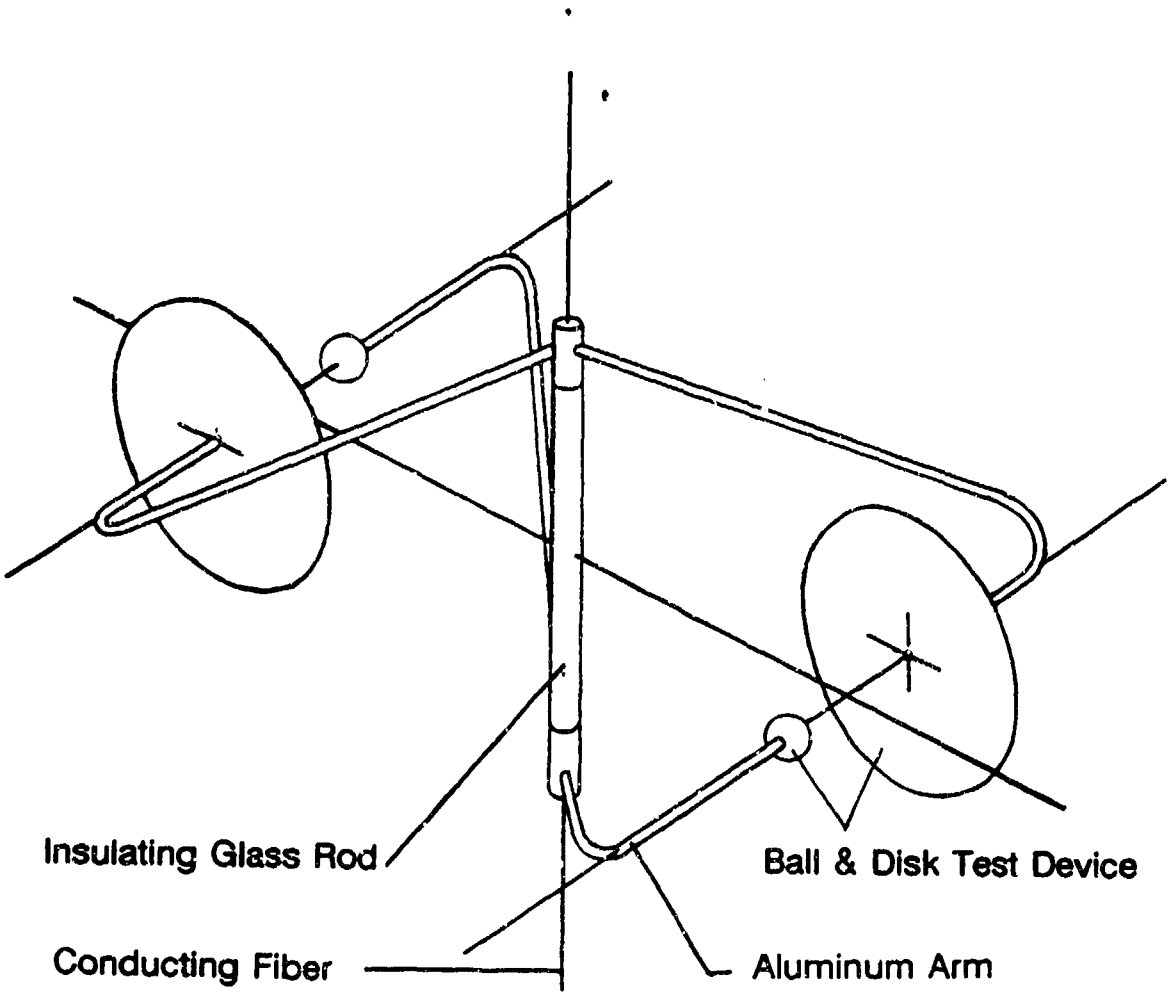

Figure 3. Test Device Support Structure

Because surface electrical breakdowns over the glass rod were experienced, this rod was replaced first with an acrylic support rod of the same size. Since the breakdowns persisted, this rod was then replaced with composite insulating separation structure consisting of a series of four fire-polished Pyrex glass petri dishes, 52 mm diameter by 16 mm high, each separated by a 12.7 mm diameter acrylic plug approximately 23 mm high. This entire central insulating structure was approximately 13 cm high with an insulating path length over the surface between the upper and lower electrodes of about 39 cm. The structure was held together with alkyl cyanocrylate instant glue, such as Krazy Glue$_R$ or Super Glue$_R$. Initially, this insulating structure enabled potential differences of about 40 kV to be obtained without breakdown, but after some use only values of about 20 kV could be maintained without breakdown.

Metal torsion fibers were of special interest for use in this program because of their electrical conductivity and their planned use as electrical leads to power the test devices. Metal fibers are known to have long term drift problems. Our approach to this drift problem was to correct for the drift over the relatively short time period of about an hour during each individual test. To do this, it was necessary to make zero angular position readings of the torsion fiber system (when the force generating electrical inputs were turned off) before, and after application of one or more voltage steps during each test. This permitted any appreciable drift of the zero position to be evaluated, and corrections to be applied to the force generated angular deflections observed during a test run.

Some drift was observed in the tests noted in References 1 and 2, but was not a serious problem. In this program, the zero drift of the torsion pendulum equilibrium position was very small and was readily correctable. In Reference 2, it was also found that large voltage increments sometimes caused shift in the

equilibrium position of the torsion pendulum, but small increments up to about 500 V left the zero position unaffected. These observations were interpreted as a problem with the rise rate (or ramp) of the voltage increment, rather than with the magnitude of the increment itself. A variety of magnitudes of voltage steps and rates of voltage rise to achieve these steps were explored experimentally. It was found that voltage ramps up to about 500 V/sec caused no appreciable drift or shift problems, and this rate was used subsequently in most tests. The maximum voltage rise rate for the driving power supplies was set at 12 kV/sec.

The torsion fiber chosen for use in this program was a 99.98% pure tungsten fiber, 0.1 mm (0.004 in) in diameter. Selected mechanical properties of tungsten fibers are given in Table 1[3][4]. Typically, the fiber strength becomes the limiting mechanical factor for each candidate fiber material and determines the corresponding minimum fiber diameter. Tungsten is one of the strongest metal fibers, and the tungsten fiber chosen is estimated to support a static load of about 0.57 kg. The upper fiber length was 0.4282 m (16.86 in), and the lower one was 0.4001 m (15.75 in).

In implementing the dual torsion fiber system the upper end of the top fiber was fastened to a vacuum sealed adjustable rod, which could be raised, lowered, or rotated manually from outside the chamber to achieve a suitable device height or angular equilibrium position for tests.

The height adjustment feature for the fiber support rod involved mounting the rod on a precision rack and pinion slide mechanism. In use, this unit was coupled with a dial indicator, and height settings and resettings to a precision of $\pm$ 0.0013 cm ($\pm$ 0.0005 in) were achievable. An azimuthal angular scale was fastened to the chamber, concentric with the movable fiber

Table 1. Selected Mechanical Properties of Tungsten Fibers

Youngs Modulus, E, N/m^2	34×10^{10}
Rigidity Modulus, G, N/m^2	13.5×10^{10}
Tension yield, N/m^2 (psi)	6.89×10^8 (100×10^3)
Density, g/cm^3	18.6-19.1

support rod. A pointer attached to the movable rod was used together with this azimuthal scale to indicate the angular position of the rod and, hence, the top of the upper fiber. Such angular position settings and resettings could be made with a precision of about $\pm$ 0.3 degrees, although the equilibrium position itself at any particular setting of the top fiber could be determined much more accurately.

As noted, the lower fiber extended from the device holder to a special attachment near the bottom of the chamber, which was designed to provide a near constant tension on both fibers. This lower fiber attachment scheme was configured to minimize the changes in the axial forces on the fibers and, hence, the fiber calibration, induced by thermal expansion or contraction of the overall vacuum chamber itself.

Further, the attachment scheme permitted the zero angular position of the dual torsion fiber combination to correspond to a zero torsion equilibrium condition of the fiber (such as would occur automatically in a single-fiber system) rather than to correspond to just a zero net torsion condition. The latter would arise if the bottom end of the lower fiber were twisted away from a no torsion position during attachment. The zero net torsion condition itself could be quite usable for a pair of fibers of equal length, and would not be expected to change the system's torsion calibration as long as the swing amplitude of the pendulum remained completely within the linear torque-twist

region of the fibers. This feature will become clear by noting that a fiber pair attached with an initial twist, would upon swinging in one direction cause a further twist to develop in one fiber of the pair and a relaxation of twist to occur in the other. For fibers of equal length, the resulting torques would still sum to the same total. Inasmuch as it was not convenient to use equal length fibers within our vacuum chamber, and the bounds of the linear torque-twist region were not well established, we preferred to use the zero torsion equilibrium conditions of the fiber, rather than the zero net torsion conditions, in the experimental work under this program.

The special fiber tensioning attachment fastened to the lower fiber near the bottom of the chamber is shown schematically in Figure 4. This unit consisted of a inner piston-like cylindrical mass, which was secured to the lower fiber and was free to slide axially between upper and lower stops within an outer cylinder-like mass element. The inner mass was also restrained by a pin in a vertical slot so this mass was not generally free to slide angularly within the outer cylinder about the fiber axis. The pin clearance of $\pm$ 0.0025 cm ($\pm$ 0.001 in) in the slot, at the inner mass radius of 0.625 cm (0.25 in), could have theoretically allowed the angular position of this mass to be uncertain by $\pm$ 0.23 degrees. In practice, the friction between the two masses was adequate to prevent the inner mass from moving during oscillations of the pendulum.

To ensure positive electrical contact between the two conducting mass elements, a very fine, loosely coiled copper wire was attached between the bottom of the piston-like component and the lower end of the surrounding cylinder. Electrical connection of the cylinder element with the conducting platform on which the cylinder rested when in place for a test, was by direct mechanical contact.

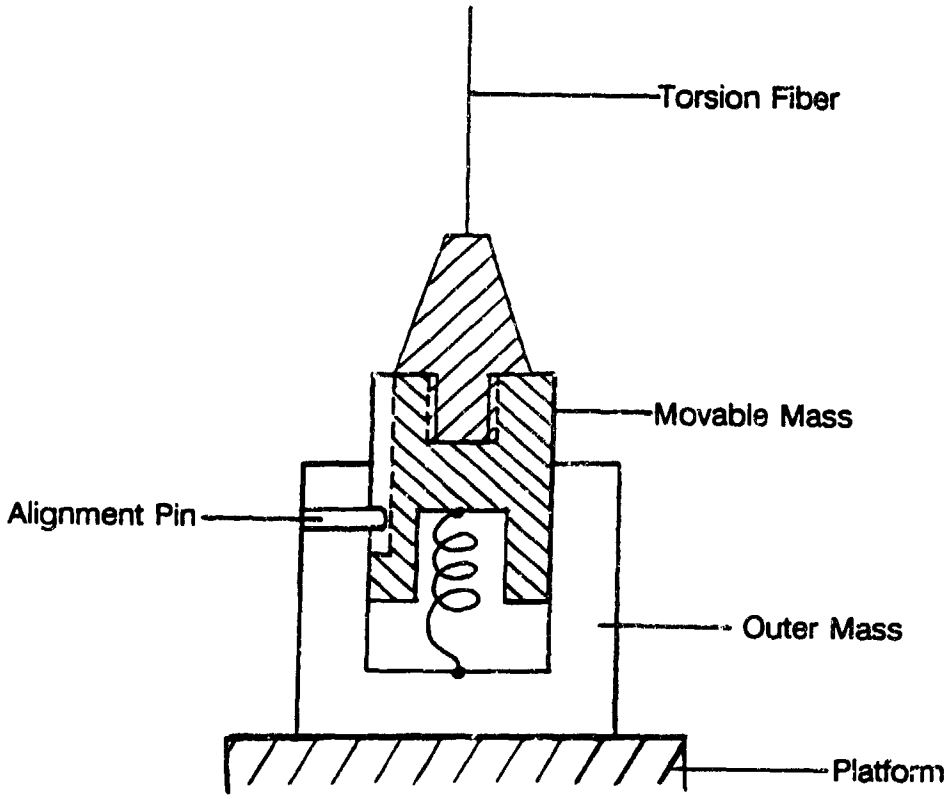

Figure 4. Fiber Tensioning Device

This fiber tensioning unit was used in conjunction with the height adjustment feature to set, and reset, the azimuth of the zero equilibrium position of the torsion fiber pendulum with respect to the chamber. The fiber was raised, without breaking the vacuum seal, until the lower composite mass was totally free from its bottom support. The top fiber was then rotated a known amount by turning the height adjustment rod in relation to the azimuthal scale of the top of the chamber. The pendulum oscillations induced by this action were then allowed to totally subside.* The fiber was then lowered so the composite mass again rested on the lower support platform. The inner mass was then raised about 2.5 mm (0.10 in) without lifting the outer element of the composite mass from the platform, so the inner mass element was suspended by the lower fiber. Thus, the weight of the inner mass again caused tensions in the upper and lower fibers to return to essentially their original values before the repositioning.

Optical Readout and Data Acquisition Subsystems

A readout subsystem consisting of a simple telescope, two mirrors and two scales was used to determine the average angular deflection of the pendulum and, hence, the corresponding twist of the dual torsion fiber system during tests. An alignment telescope equipped with a cross hair reticle was directed to view, via reflection from one of two mirrors oriented near right angles to each other, one or another of two linear scales mounted on the inside wall of the chamber. A definite reading could then

---

* Such pendulum oscillations damped very slowly under high vacuum conditions, sometimes requiring two to three days. Later in the program it was found that the overall time could be shortened very simply by increasing the chamber pressure to about 10^{-3} torr, letting the pendulum come to rest, and then pumping the vacuum back to about 10^{-6} torr. This cycle time typically required less than one day. In retrospect, it is recognized that more direct damping techniques could have been used.

be determined at the intersection of the cross hair with the scale image. Because the optical path used included a reflection from a mirror, the apparent deflection read through the telescope directly from either scale on the chamber wall corresponded to exactly twice the angular rotation of the pendulum.

Each linear scale consisted of three stainless steel, flexible machinist's scales 0.6096 m (24 in) long with subdivisions in English units of 1/50 in. These machinist's scales were carefully welded together at the ends to make each linear scale continuous. One such complete scale was mounted just above the telescope viewing port and was viewed using one mirror. The second complete scale was mounted below the telescope viewing port and was seen using the second mirror, oriented near 90 degrees in azimuth about the fiber axis from the first mirror. The scales were sufficiently long to permit both to be seen simultaneously using one of the mirrors. This permitted the scales to be compared, and readings taken on one scale to be consistently converted to that of the other. Thus only one set of final scale readings were employed.

In this arrangement the radial distance, r, from each mirror to its corresponding scale was 0.5175 m (20.38 in).

For convenience in testing, the extremes of the apparent angular deflection (expressed as scale readings), rather than continuous or other periodic values during complete oscillations of the pendulum, were recorded as data. By averaging the extremes, the positions of the centers of oscillation were determined both when an applied torque was present and when it was absent. The differences between these averages gave the deflection of the pendulum associated with the applied torque.

Each scale was typically read to the nearest 1.27×10^{-4} m (0.005 in), and the central position of each individual

oscillation measure was determined to the same degree of uncertainty. A typical force measurement during a test involved about ten oscillations, so the calculated uncertainty of the mean was about 0.40×10^{-4} m (0.0016 in). However, taking into account reading uncertainties and system noise, a somewhat larger deflection of about 0.64×10^{-4} m (0.0025 in) is believed to be representative of the threshold of measurements. This results in a minimum deflection angle of the mirror

$$\theta_{min} \approx 6.14 \times 10^{-5} \text{ radian per 0.0025 in apparent motion of the scale.}$$

This value of θ_{min} corresponds to about 13 seconds of arc, which is not of great sensitivity, but is about four times better than was achieved under the Phase I program.

During the initial set-up of the propulsion device tests some observations were made visually through the telescope. The preferred technique employed in essentially all routine test runs involved using a video camera and monitor, with the camera lens positioned to see through the telescope eyepiece. Deflection readings during tests were then made directly from the video monitor. These were entered manually into a computer, after first pressing a single key to record the time (supplied by the computer) to which each reading corresponded.

A General Electric VHS movie Video System SE9-9108 with video tape recorder was used for most of the test runs. Use of the recorder permitted a real time record of the actual test run to be made. This record was helpful since it permitted replaying the test run to confirm deflection readings or to ascertain missed readings after-the-fact.

Readout of the pendulum oscillations for torsion fiber calibration--carried out by measuring the swing periods of the

fiber as part of a torsion pendulum--required a different approach from the video camera technique used during force measurement tests. This is because the swing time periods cannot be determined visually with sufficient accuracy. In this case, a pendulum bob of known mass, geometry, and moment of inertia was used with the fiber to be calibrated, in place of the actual test devices and their support structure. The same telescope and mirror system was again used, but an active signal in the form of a laser beam was passed through a beam splitter, through the telescope, and onto the mirror. Twice each period as the mirror oscillated, the laser beam was reflected back through the telescope, into the beam splitter and deflected into a fiber optic cable and then onto a photo detector and amplifier. Real time electrical signals from the detector amplifier were sent to a digital oscilloscope and recorder, where the signal pulses were displayed and timed accurately.

For the calibration runs, the zero angular position of the torsion fiber and mirror was adjusted so the laser beam was reflected into the detector when the pendulum passed close to its equilibrium position. Near this position, the angular deflection rate of the mirror was the greatest, and the duration of the optical pulse at the photodetector was close to a minimum. This facilitated making accurate measurements of the instant when the pulse occurred (usually reckoned at the maximum amplitude of the pulse).

The actual system assembled used a Spectra Physics type 155A, 0.5 mW, helium-neon laser; a 10 mm x 10 mm prism beam splitter; a plastic fiber optic light guide; a photodiode detector with an IC instrumentation amplifier designed and built at Veritay; and a Nicolet Digital Oscilloscope Model 2090 with disk recorder.

Typical digital sampling times used were 0.05 sec per point. At this sampling rate, a total sample of $32x10^3$ points (26.7 min) could be recorded directly. The total time used for calibration runs encompassed about eight to fifteen complete oscillation periods.

Electrical Subsystem

The high voltage sources to drive the devices under test consisted of a pair of Spellman regulated, 0-60 kV, DC power supplies, Model UHR60PN30, each of which had a maximum power output of 30 watts. The voltage polarity of each supply was reversible internally, but was not directly switchable for safety reasons. These two separate high voltage power supplies could be grounded at a common earth ground and operated "back-to-back," with one providing a negative voltage and the other a positive voltage. This enabled one electrode of each test device to be set at an arbitrary positive potential with respect to ground, and the other electrode to be set at a selected negative potential. This also allowed complete flexibility in setting the potentials of the device electrodes relative to the grounded chamber.

The high voltage was fed from the supplies to the test chamber and devices using high voltage cables, each rated with a DC breakdown voltage of 100 kV. Lesker VZEFT-10, 50 kV electrical feed throughs, configured for vacuum operation, were used to bring the high voltage into the vacuum chamber.

In this program, we chose to operate and control the high voltage supplies, together with two electrometers used for the measurement of combined current through the two test devices, with an IBM XT computer. Several advantages were associated with this choice, but the main ones were: (1) to permit software changes rather than hardware modifications in this part of the

system as certain test requirements and procedures varied; and (2) to enable the high voltage power to be applied to the test devices in a repeatable fashion from test to test without manual manipulation.

In addition, the computer used for this control also functioned as a data logger. Data from both the power supplies and the electrometers, along with information entered from the keyboard, were automatically stored in a random file during each test. Hardcopy results in tabular or graphical format from this file were readily produced subsequent to each test run.

The programmed variables for the high voltage supplies included voltage output levels, and time rates of voltage change (rise and fall) for reaching these levels.

To implement this approach both power supplies were first modified internally for remote operation. The XT computer was then outfitted with two peripheral boards to provide the necessary I/O capabilities for controlling the two systems. One I/O device was used to handle voltage program levels and monitoring of both high voltage supplies; a second I/O device, specifically designed by Veritay, was used to handle 16 bit serial data from each electrometer. A block diagram shown in Figure 5 illustrates the connection of both the high voltage supplies and the electrometer to the computer system.

The high voltage program and feedback levels were managed by an analog and digital interface board, model DASCON-1, from Metra Byte Corporation. This board allowed full range programming of both power supplies (0 to 60 kV) in 15-V increments using the two on-board digital-to-analog (D/A) converters. In addition, the multiplexed A/D converter, also on-board, provided the voltage and current feedback required to maintain proper and safe automatic operation of the supplies.

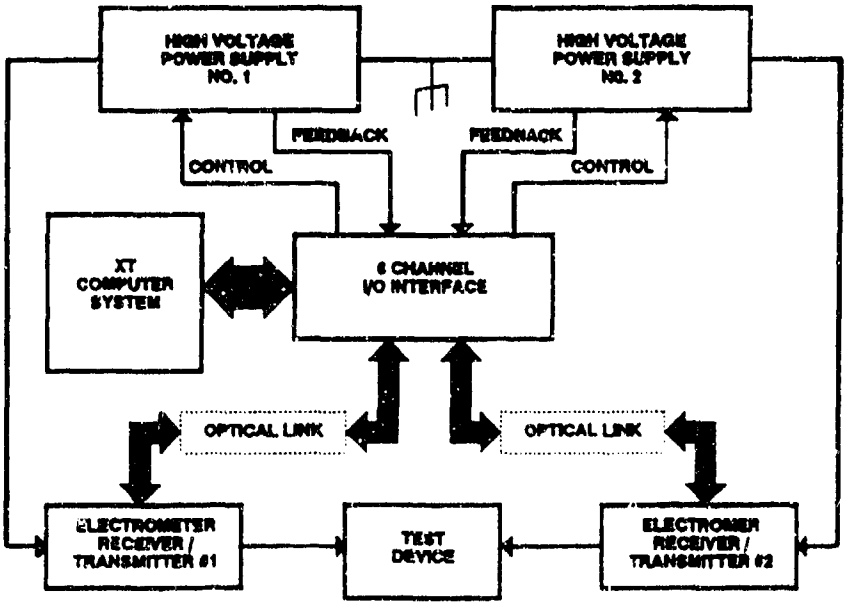

Figure 5. Block Diagram of High Voltage Control and Current Data Acquisition

A complete test could be preset into the computer using the associated control and data logging software. Program flow evolved around several loops and interlocks to ensure that data acquisition was continuous for inputs from both the keyboard and the I/O board, while the power supply settings were changed automatically or by manual activation. Safeguards and various visual annunciators incorporated in the program apprised the test operator of problems, such as high voltage breakdown or lost communication with I/O devices. The system also had the capability of complete shutdown in the case of failure of a key component.

The instrumentation to measure low level electrical current through the test devices was specifically configured to accommodate the high voltage of interest, to minimize losses, and to operate inside the vacuum chamber as close as possible to the test devices. A two-current sensor system was used, one to sense the current in the upper conducting torsion fiber, and the other in the lower fiber. Each such sensor unit had a set of components inside the chamber and another set outside. Each inside sensor set was designed as a miniaturized, self-contained battery powered unit which could operate electrically isolated at the level of the high voltage input to the test devices. The inside set consisted of an electrometer with an A/D converter, an electrically isolated battery power supply, and an electro-optic transceiver. The outside set consisted of another electro-optic transceiver, an I/O interface board, and the same IBM XT computer used with the high voltage power supplies.

A functional diagram of one of the two identical electrometer transceiver circuits is shown in Figure 6. A twelve-bit A/D converter and an FET-input electrometer amplifier form the base of the circuit. Additional opto-electronic circuitry was used to achieve high voltage isolation and serial communication with the electrometer I/O interface noted earlier. The amplifier, configured as a current to voltage converter, provided a full scale output of $\pm$ 3.000 V. This corresponded to a full scale input current of $\pm$ 3.000 nA. The instrument contained three other on board voltage sources, two of which were a circuit ground, and a 1.23-V precision voltage reference. These were primarily used for calibration purposes and to check on the overall accuracy of this electrometer. The third source was a 9-volt battery supply to power the overall electrometer-transceiver (ET).

To help preserve battery life, an automatic shut-off feature was added to put the ET unit in a stand-by mode of operation

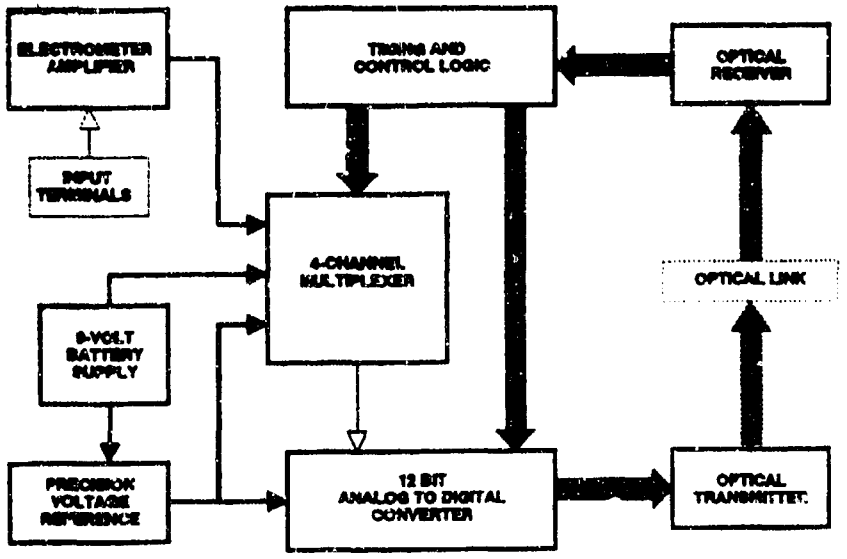

Figure 6. Functional Diagram of Electrometer-Transceiver

while it was not in use (i.e., when it was off line with the computer system). This disabled all but the photodiode receiver circuitry. This was a necessary feature as frequent battery replacements were not feasible around the sensitive torsion fiber--- where the ET unit was located. The ET unit on stand-by could be reactivated by a "wake-up" signal generated by the (outside) I/O interface and sent as an optical signal from the outside transceiver to the inside one. In the standby mode, the circuit exhibited minimal draw on the power source--approximately 1/50 of the maximum quiescent current drain of the entire unit--and thus extended battery life.

The accuracy of each electrometer unit was assessed by observing/calibrating the electrometer input/output

characteristics prior to installation in the vacuum chamber. This action was performed using known current level inputs and comparing the output using a Fluke digital voltmeter. Error correction factors were determined and compensation was applied, using computer software, thereby eliminating the need for additional circuitry. The overall accuracy obtained was estimated to be within 0.1 percent.

Each electrometer transceiver unit was installed in a stainless steel enclosure, as shown in Figure 7. One such enclosure is located at the upper end of the top torsion fiber; the other near the lower end of the bottom fiber. The electrometer was fabricated on a flexible printed circuit board, which was situated with its major electronic components against the inside wall of the steel shell. This provided additional shielding as well as a heat sink for the A/D converter and for the electrometer amplifier---a relevant consideration in a vacuum environment. A sealed acrylic case housed the 9-volt lithium battery used as the main power source; this plastic case also served to contain any cell leakage that might have occurred, thereby minimizing the risk of vacuum chamber contamination. Electrical connections between the circuit board and the test device were made using a double-sided conductive plate. The plate itself was easily slipped into spring loaded contacts at the upper and low termination locations of the torsion fibers. The optical link between inside and outside ET units was made through plastic optical fibers. This use of optical isolation helped overcome severe problems of electrical insulation, losses and chamber wall pass-through that would otherwise have been associated with direct electrical wiring.

Vacuum Subsystem

The vacuum system used for tests is shown schematically in Figure 8. It consisted of a CVC Model PAS-66D expanded 6-inch

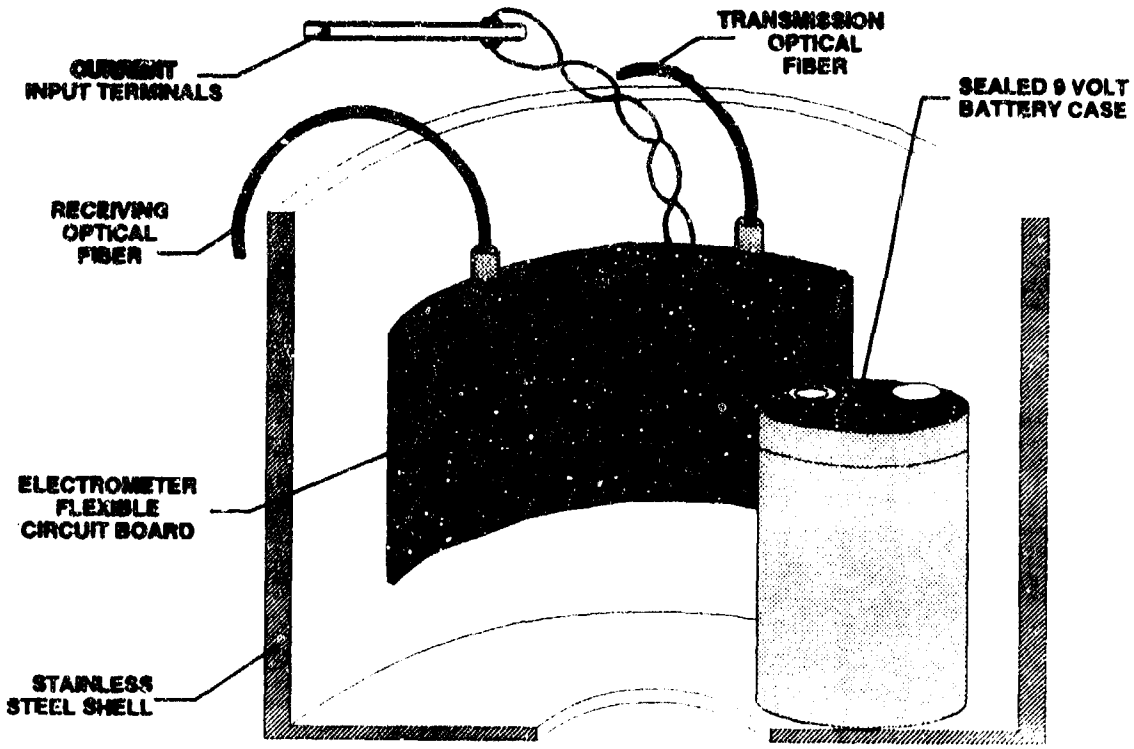

Figure 7. Electrometer-Transceiver Configuration

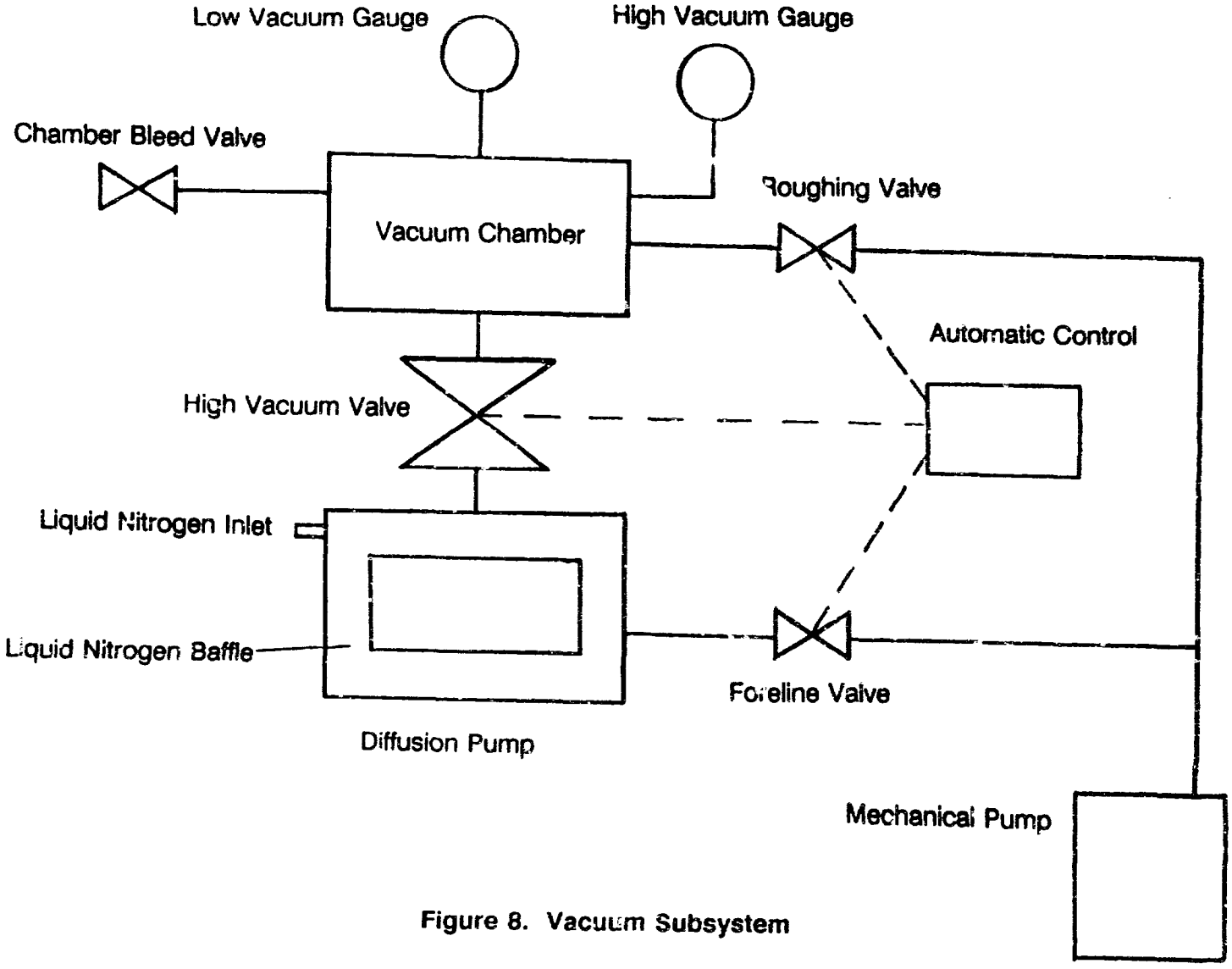

Figure 8. Vacuum Subsystem

diffusion pump with liquid nitrogen baffle, automatic valves, an automatic valve controller, a hot filament ionization vacuum gauge, and a Kinney KTC-21 (21 CFM) two-stage backup vacuum pump. An Edwards Pirani gauge head PRM 10K with controller was also used a backup low vacuum gauge for the chamber. A Labconco McLeod gauge was also available for calibration checks of the Pirani gauge and the mechanical backup pump.

The ultimate pressure rating of the backup pump was 2×10^{-4} torr. When it was connected to and pumping the chamber (prior to activating the diffusion pump) the vacuum typically did not reach the ultimate value indicated, but it was below 10^{-3} torr and performed well.

The diffusion pump also performed admirably, and after cycling the system with dry nitrogen gas in the chamber to help remove water and other residual gases, and pumping for a few days to overcome some minor outgassing, vacuum levels below 10^{-5} torr were achieved. As the test work continued, vacuum levels of 10^{-6} torr were obtained routinely, and levels down to about 5×10^{-7} torr were obtained occasionally.

Test Devices

Six candidate test devices that were used for propulsion tests are shown schematically in Figure 9. Some of these device types are representative of the various electrically driven devices which T.T. Brown investigated in an attempt to produce thrust [5]. Others represent variations from Brown's units, selected to probe the differences between symmetric and non-symmetric devices. The devices are numbered to facilitate referring to them in the experimental investigations. The construction materials and device dimensions are given in Table 2.

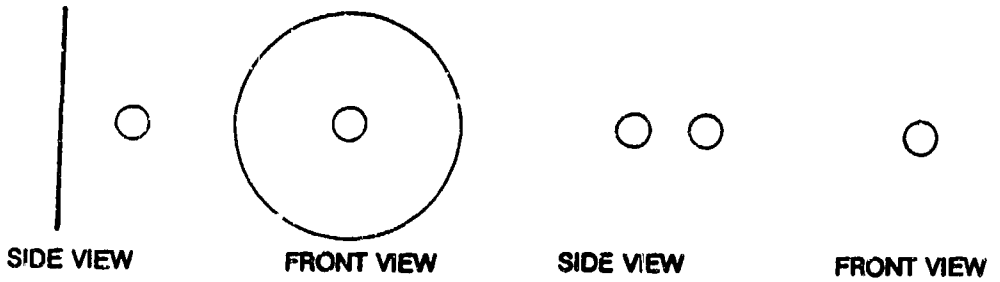

No. 1 Ball and Plate

No. 4 Symmetric Ball

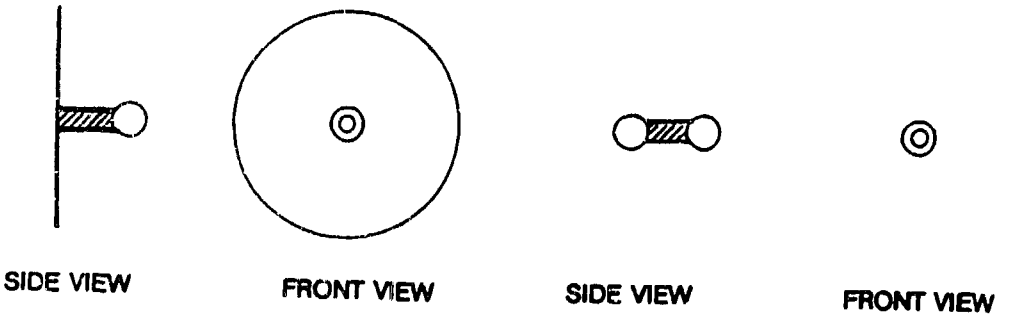

No. 2 Ball and Plate With 1/4-Inch Diameter Dielectric

No. 5 Symmetric Ball With 1/4-Inch Diameter Dielectric

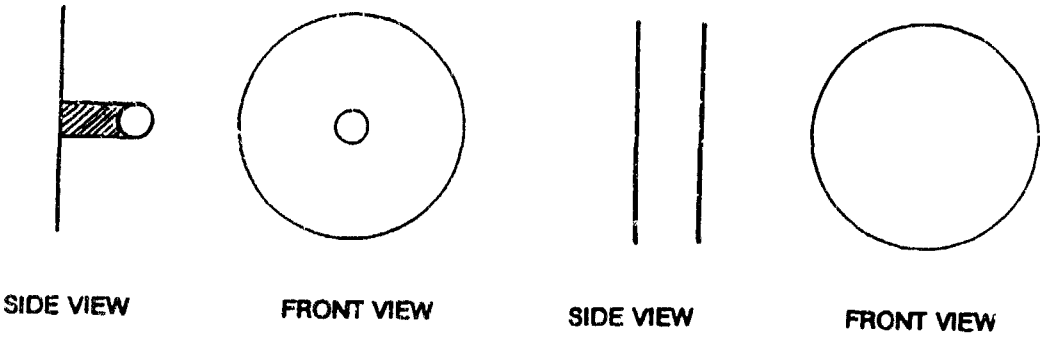

No. 3 Ball and Plate With 1/2-Inch Dielectric

No. 6 Symmetric Plate

Figure 9. Test Device Types

Table 2. Characteristics of Devices Used in Propulsion Tests

Device No.	Component	Material	Diameter (m)	Thickness (m)	Electrode Separation m(in)
1A	Ball	Aluminum	0.0127	--	0.0483 (1.900)
	Plate	Brass	0.0793	0.00038	--
1B	Ball	Aluminum	0.0127	--	0.0190 (0.750)
	Plate	Brass	0.793	0.00038	--
2	Ball	Aluminum	0.0127	--	--
	Plate	Brass	0.0793	0.00038	--
A	Dielectric	Acrylic	0.00635	--	0.0483 (1.900)
B	Dielectric	Acrylic	0.00635	--	0.0190 (0.750)
C	Dielectric	**NOTE 1**	0.00635	--	0.0161 (0.635)
3	Ball	Aluminum	0.0127	--	--
	Plate	Brass	0.0793	0.00038	--
	Dielectric	Acrylic	0.0127	--	0.0190 (0.750)
4	Ball (2)	Aluminum	0.0127	--	0.0127 (0.500)
5	Ball (2)	Aluminum	0.0127	--	--
	Dielectric	Acrylic	0.00635	--	0.0127 (0.500)
6	Plate (2)	Brass	0.0793	0.00038	0.0229 (0.900)

NOTE 1: Lead titanate-lead zirconate piezoelectric

It will be noted that Test Device Type No. 2 was configured for different tests with two different types of dielectrics, acrylic and lead titanate-lead zirconate.** The dielectric constant of the former is about 3.5, and the latter is about 1750.

The basic ball and plate unit was a device type used extensively by Brown, and apparently with some success in generating propulsive forces. While the devices Brown used normally included a dielectric, the devices tested here were configured both with and without dielectrics. A key feature of this test unit, according to Brown[5] is that it would develop a nonlinear electric field between the ball and plate.

The symmetric ball, or symmetric plate, test devices were expected to develop symmetric electric fields between the electrodes and, again according to Brown [5], should generate minimal or zero propulsive forces.

TEST RESULTS

Test Approach

The overall test approach emphasized the direct measurement of propulsive forces under high vacuum conditions. Direct force measurements were considered essential since the nature and characteristics of the forces under investigation were unknown. From the space propulsion point of view, the very existence of this propulsive force in a vacuum was of key interest. A known phenomenon called electrical (or ion) wind has frequently been

---

** This is a piezoelectric ceramic material designated Channel 5500 by its manufacturer, Channel Industries, Inc., Chesterland, OH 44026.

invoked as a mechanistic basis of thrust on electrostatic-driven propulsion devices similar to, and including, those explored by Brown. Electrical wind does, in fact, contribute to the thrust on such test devices when they operate in air. In a vacuum, another force contribution, known as ion propulsion, is known to be operative, but is usually quite small unless very large electrical currents or current pulses are used. This ion propulsion results from a transfer of momentum to the body of a test device (or an ion engine), as a result of the electrical ejection and acceleration of ions unidirectionally from an ablative source within the engine.

At the outset of this program a choice was made to drive the test devices using steady electrostatic potential differences between the electrodes of the devices. Generally, it was also understood, on the basis of Brown's comments (Reference 1, page 8 and Reference 5) that the thrust existed under high vacuum conditions," when there was no vacuum spark." (A vacuum spark--or breakdown--might have been adequate to account for the thrust just on the basis of the ion propulsion effect alone.) Near the very end of this program, we briefly examined the force generation effects with pulsed fields, under near breakdown conditions. The overall test set-up for this program was configured in accord with the primary choice to drive the test devices with DC voltages. An alternate configuration would likely be more appropriate for a non-DC voltage drive.

With this constraint, a principal concern and unknown for the test effort was the influence that the tank wall boundaries might have on the forces exhibited by the electrostatically driven test devices. Two means were employed to examine the influence of tank wall boundaries. The first, and simplest scheme, used two mirrors oriented at right angles to each other and mounted on the test device support. This, together with the scale mounted on the vacuum tank wall and the ability to reset

the zero equilibrium position of the torsion pendulum to any azimuth, permitted force measurements to be made at various equilibrium positions over a 180 degree range. This range was commensurate with one full angular period of the two-device support structure. The force measurements, in turn, made it possible to detect any significant asymmetries in the total force on the test devices.

The second scheme employed a 0.20 m (8.0 in) square "boundary plate" fastened to a vacuum-sealed movable rod and located inside the chamber. The rod and plate were electrically grounded to the chamber wall and could be positioned from outside the tank, so plate was at a given radial distance from the wall. The objective of using such a plate was to determine whether the plate introduced asymmetries in the force measurements as a function of relative azimuthal position of the test devices and plate. Also it was used to determine whether such boundary effects would disappear as the plate approached the tank wall.

Calibration

Calibration of the dual torsion fiber system was carried out by measuring the period of the torsion pendulum, consisting of the fibers, a calibration mass (which was substituted for the test devices and their support structure) and the mirror holder.

Results for the pair of fibers used throughout the tests are given in Table 3. The torsional stiffness, S, of the fiber pair operating as a system was calculated using the equation

$$S = \frac{Q}{\theta} = I\frac{4\pi^2}{T^2}, \qquad (1)$$

where

Q = total torque; N-m

θ = angle of twist of the calibration mass and mirror and, hence, of each fiber; rad

I = moment of inertia of the suspended mass; kg-m^2

T = oscillation period; s.

An analysis of a damped oscillating torsion pendulum[2] has indicated that the true value for the torsional stiffness, S, given by equation (1) requires the use of the period T_o of oscillation of the undamped pendulum. However, it is known that the dual fiber system used here operated as a damped oscillating torsion pendulum, and it was assumed to be driven by a time-independent force pulse, which acted over several oscillation periods. The damped oscillations of this type of system are mathematically not periodic functions, but they do exhibit a consistent conditional period, T_1. It is this conditional period T_1, which is measured to determine S. It is necessary to examine the relationship between these two periods in order to determine an accurate value for S.

The oscillation of such a damped pendulum can be characterized for the present application by only two quantities:***

*** In general, two more quantities are required: the conditional amplitude, K, for a given time, and the phase angle α of the various components which comprise and characterize the oscillations (see Reference 6).

Table 3. Calibration of Dual Torsion Fibers

Fiber Pairs:

Fiber:	Tungsten
Diameter, D:	0.010×10^{-2} m (0.004 in)
Length (Top), L_T:	42.82×10^{-2} m (16.86 in)
Length (Bottom), L_B:	40.01×10^{-2} m (15.75 in)
Cross Sectional Area, A:	7.854×10^{-9} m (1.257×10^{-5} in^2)

Total Calibration Pendulum:

Mass, M_c, kg:	0.10416
Moment, I_c, kg-m^2	1.2805×10^{-5}

Data:

Test No.	1C	2C	3C	4C	5C	11C
No. Periods	16	16	15	16	15	15
Temp. °K (°F)	288.7(60)	288.7(60)	285.9(55)	285.9(55)	288.7(60)	295.4(72)
Vacuum, Pa (Torr)	$2.0X10^{-3}$ ($1.5X10^{-5}$)	$4.0x10^{-1}$ ($3.0x10^{-3}$)	$1.33x10^{1}$ ($1.0x10^{-1}$)	$1.33x10^{2}$ (1.0)	$1.01X10^{5}$ (760)	$1.33x10^{-1}$ ($1.0x10^{-3}$)
Swing Period, s	8.9164	8.9162	8.9133	8.9094	8.9200	8.9267
$\pm$ 1σ, s	0.00483	0.00329	0.00469	0.0124	0.00681	0.0110
$\pm$ 1σ, %	0.054	0.037	0.053	0.139	0.076	0.123
Torsional Stiffness S, N-m	$6.3587x10^{-6}$	$6.3595x10^{-6}$	$6.3612x10^{-6}$	$6.3688x10^{-6}$	$6.3560x10^{-6}$	$6.3441x10^{-6}$

S as function of Temp., N-m

$$S = [-0.001181\ (T_{.F}) + 6.4290] \times 10^{-6}$$
$$S = [-0.002126\ (T_{.K}) + 6.9719] \times 10^{-6}$$

Calculated Rigidity Modulus, G, N/m^2 13.38×10^{10} at 20°C

T_1, the conditional period of oscillation, which represents the time between consecutive zero amplitude crossings in the same direction (this also corresponds to the conditional angular frequency ω_1).

d, the logarithmic decrement, a dimensionless measure of the damping, which is the natural logarithm of the ratio of angular displacements one period apart. It is related to the conditional period, T_1, and the damping coefficient h, and the pendulum swing amplitudes $\theta(t)$ by

$$d = T_1 h = \ln \frac{\theta(t)}{\theta(t+T_1)} . \qquad (2)$$

From the relation[6]

$$\omega_1^2 = \omega_0^2 - h^2 ,$$

where h is the damping coefficient, and ω_0 and ω_1 are the respective angular frequencies for the undamped and damped oscillations, S can be expressed as

$$S = I\,\omega_0^2 = I\,\omega_1^2 \left[1 + \left(\frac{h}{\omega_1}\right)^2\right]. \qquad (3)$$

These angular frequencies, in turn, are related to the oscillation periods by

$$\omega_o = \frac{2\pi}{T_o} \qquad (4)$$

and

$$\omega_1 = \frac{2\pi}{T_1} . \qquad (5)$$

The measured value of h for the dual torsion system with tungsten fibers was about 5.0×10^{-5} s^{-1}. The ratio $(h/\omega_1)^2$, which was approximately 2.2×10^{-7} for the devices tested and smaller for the calibration mass used, was, therefore, negligible in Equation (3). In turn, S was adequately approximated using Equation (1) with $T = T_1 \approx T_0$.

From the Phase I work, it was learned that the effect of temperature on the fiber calibration values was apt to be significant. The variation in torsional stiffness, S, of the dual tungsten fiber system with temperature is shown in Figure 10. The points indicated in this figure correspond to the data from Table 3, except the values at the two highest pressures for test numbers 4c and 5c were not used. As a result, the calibration curve in Figure 10 corresponds to vacuum levels over the approximate range of 13.3 Pa (1×10^{-1} torr) to 1.33×10^{-4} Pa (1×10^{-6} torr). At 20°C (68°F) the temperature coefficient measured for the torsional stiffness is -0.033 percent per degree Celsius increase (-0.019 % /°F).

The rigidity modulus, G, for the fibers in each pair were assumed to exhibit the same value, since this modulus is characteristic of the fiber material and geometry, and since the fibers were cut from a single longer length of material.

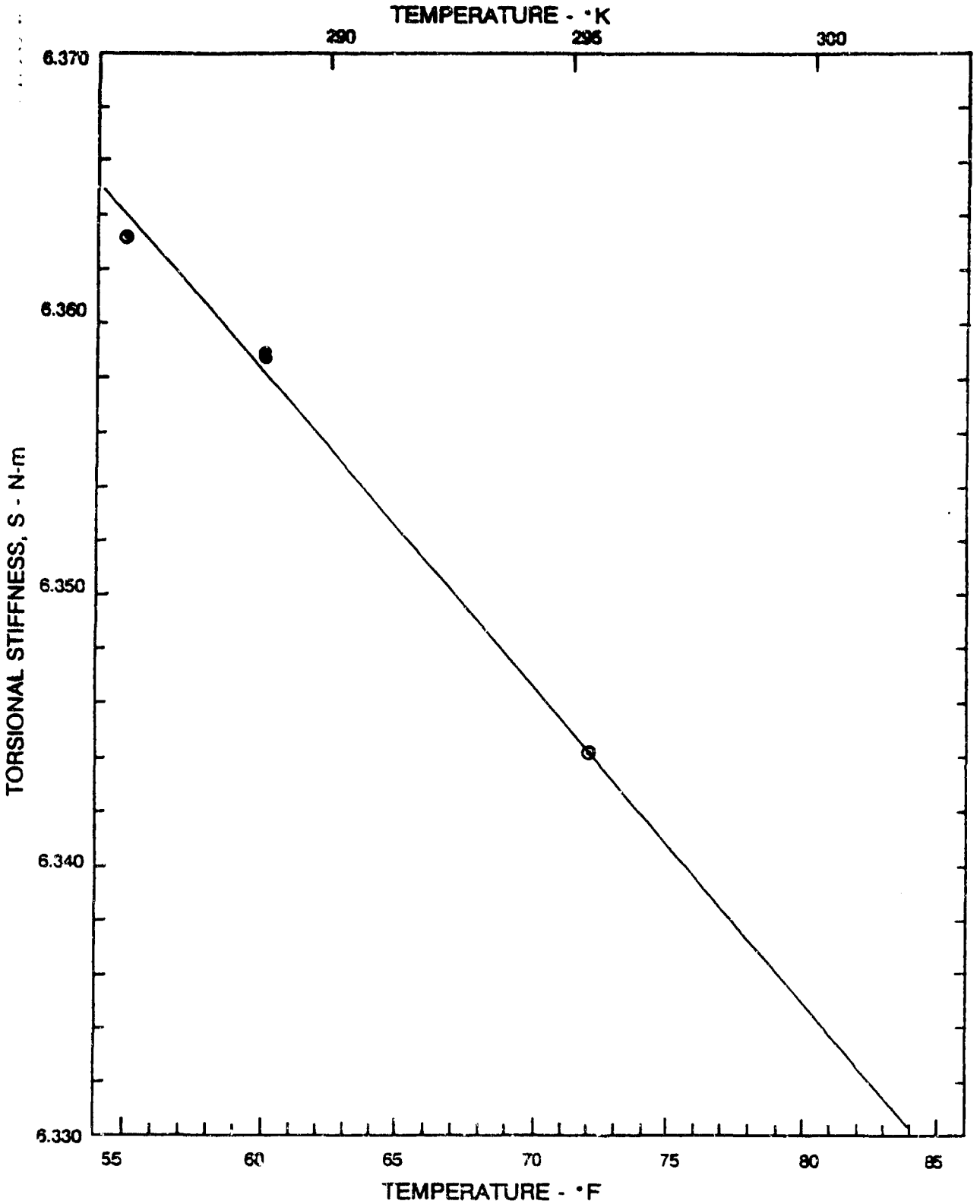

Figure 10. Tungsten Torsion Fiber Calibration

For a single fiber, the rigidity modulus is related to the torsional stiffness, S, by

$$S = \left(\frac{GA^2}{2\pi L} \right), \qquad (6)$$

where

A = fiber cross sectional area

L = fiber length.

For the dual fiber system, the total torque Q, acting on the device holder which joined the top and bottom fibers near the chamber center, was the sum of torque contributions Q_T, from the top fiber and Q_B from the bottom. In this case, the angle of twist θ for each fiber was the same, so that

$$Q = S\theta = \left(\frac{GA^2}{2\pi} \right) \left[\frac{1}{L_T} + \frac{1}{L_B} \right] \theta .$$

Then

$$S = \frac{GA^2}{2\pi} \left[\frac{1}{L_T} + \frac{1}{L_B} \right]$$

or

$$G = \frac{2\pi}{A^2} \left(\frac{L_B L_T}{L_B + L_T} \right) S, \qquad (7)$$

where

L_T, L_B = lengths of the top and bottom fibers, respectively.

The rigidity modulus was calculated using Equation (7), together with the temperature dependence of S indicated in Table 3 and Figure 10, to obtain the value $G = 13.38 \times 10^{10}$ N/m^2 at 20°C. The exact temperature at which the handbook value[3] of $G_H = 13.5 \times 10^{10}$ N/m^2 was determined is not known, but room temperature (often taken as 20°C) is likely. As can be seen, the value calculated here compares favorably (within about 0.9%) with the handbook value.

The test device support unit with two mounted devices of type No. 1A was run as a torsion pendulum in order to determine the moment of inertia, I_S, of this system. Equation (1) was solved for I_S, using the known value of S for the fiber pair and the approximation $T=T_1$. Separate determinations of I_S for device 1A gave the values shown in Table 4. It will be noted that there is a significant change in the swing period and, hence, the calculated values of I_S with vacuum level. The value of $I_S = 4.4868 \times 10^{-7}$ kg-m^2 obtained for Test No. 10C at a vacuum level of 1.33×10^{-3} Pa (1×10^{-5} torr) is likely the best value, but without replication and further investigation it remains suspect.

In principle, this value (or an improved one) could have been used with this particular torsion pendulum to check or recalibrate the torsion fiber pair directly, without the need to reuse the calibration mass. This recalibration approach was not actually used, in part because of the above noted sensitivity of calculated I_S to the vacuum level, and in part because a number of different test devices were used and a relatively large number of tests would be required just to obtain the individual moments of inertia for each case. Rather, the calibration mass, itself, was reintroduced after the data runs began, to obtain another calibration point at a higher temperature, as indicated in

Table 4. Moment of Inertia Determinations

Fiber Pairs:

Fiber: Tungsten
Diameter, D: 0.010×10^{-2} m (0.004 in)
Length (Top), L_T: 42.82×10^{-2} m (16.86 in)
Length (Bottom, L_B: 40.01×10^{-2} m (15.75 in)
Cross Sectional Area, A: 7.854×10^{-2} m (1.257×10^{-5} in^2)

Total Pendulum:

Device No.	1A	1A	1A	1A	1A

Data:

Test No.	6C	7C	8C	9C	10C
No. of Periods	28	28	28	28	28
Temp. °K (°F)	(62)	(62)	(59)	(59)	(62)
Vacuum, Pa	1.01×10^{5}	1.01×10^{5}	5.32×10^{1}	2.66×10^{1}	1.33×10^{-3}
(torr)	(760)	(760)	(4×10^{-1})	(2×10^{-3})	(1×10^{-5})
Swing Period, s	53.5232	53.2545	52.9170	52.9054	52.7911
$\pm$ 1σ, s	1.88	0.396	0.0289	0.0267	0.0183
$\pm$ 1σ, %	3.51	0.743	0.0546	0.0504	0.0346
Torsional Stiffness S, N-m at Temp.	6.3558×10^{-6}	6.3558×10^{-6}	6.3593×10^{-6}	6.3593×10^{-6}	6.3558×10^{-6}
Device Moment, I_s kg-m^2	4.6121×10^{-7}	4.5659×10^{-7}	4.5107×10^{-7}	4.5087×10^{-7}	4.4868×10^{-7}

Figure 10. This recalibration test also helped confirm that this value was consistent with earlier values--even though a temperature change was involved.

It should be noted that only the moment of inertia I_s of the support with the devices needs to be known in order to recalibrate the fibers with the test device pendulum. The original fiber calibration value of S can be used to determine the force generated by any particular device pair, provided the temperature is taken into account, and the axial tension does not alter the value of S. The fact that a moment of inertia I_s was not determined for each of the device types did not preclude determining force values from deflections observed during tests with each such unit.

The force, F, on each test device was obtained directly using the expressions:

$$\theta = (x - x_o)/2r, \qquad (8)$$

$$Q = S\theta, \text{ and} \qquad (9)$$

$$F = Q/2R, \qquad (10)$$

where

x_o = zero equilibrium position of pendulum on a linear scale

x = final equilibrium position of pendulum on a linear scale

r = mirror to scale distance = 0.5175 m (20.375 in)

θ = angular deflection of mirror and devices, and angle of twist of the torsion fiber; rad

S = torsional stiffness (at a given temperature); N-m

Q = total torque on fiber; N-m

R = moment arm of each device about fiber axis; 0.09785 m (average)

F = force on each device; N.

These relations were combined into the following single expression for evaluating F:

$$F = k \cdot \Delta x, \qquad (11)$$

where

$$k = \frac{S}{4rR}, \qquad (12)$$

$$\Delta x = (x - x_o), \qquad (13)$$

and k becomes temperature dependent. This expression for F was used in reducing test data under this program.

Boundary Effects

Initially it was suspected that force measurements made with the torsion pendulum arrangement might be influenced by induced surface charges on the walls of the vacuum chamber surrounding the test devices. Since reasonable care was taken to ensure constructional symmetry in the pendulum, the device support structure, and the test devices, all with respect to the chamber axis, the main boundary effects--if any--were expected to arise from features which might upset this symmetry. This could include various ports in the chamber, the shielded cables, small protuberances on the chamber wall, etc.

Force measurement tests to check various features of the system and to explore the nature of the boundary effects are summarized in Table 5. The initial six tests were for the

Table 5. Boundary Effects Test Summary

Test No.	Date-Time Mo Da-Hour (1989-1990)	Device No.	Pressure Pa(torr)	Temp. °K(°F)	Voltage Polarities: Top (B = ball, P = plate)	Voltage Polarities: Bottom (B = ball, P = plate)	Equilibrium: Position x_0(in)	Equilibrium: Angle(x2) θ(deg)	Total Force - μ N (± 1σ, %): Voltage Between Electrodes, kV: 5	10	15	20	25	30	33	Force Toward (B = ball, P = plate) [See Note 1]	Remarks
1	11-17-1050	1A	1.15E-3(8.6E-6)	290.4(63)	+ V/2 (B)	- V/2 (P)	34.550	97.13	-0.00797	-0.03068						P	shakedown- 0°Pendulum Posit. (P.P.) Drift Check
2	11-17-1400	"	1.19E-3(8.9E-6)	292.0(66)	"	"	34.666	97.45	-0.00396	-0.02706	-0.06371	-0.1147	-0.1824	-0.2660		P	0°P.P., Drift Check
3	11-17-1500	"	1.24E-3(9.3E-6)	292.0(66)	"	"	34.713	97.59	-0.00597	-0.02429	-0.05814	-0.1063	-0.1772	-0.2606		P	0°P.P., Drift Check
4	11-27-1505	"	9.87E-4(7.4E-6)	290.9(64)	"	"	34.850	97.97	-0.01195	-0.03824	-0.08485					P	0°P.P., Voltage Steps
5	11-28-1458	"	1.07E-3(8.0E-6	290.9(64)	"	"											0°P.P., Program Error Power
6	11-29-1522	"	1.07E-3(8.0E-6)	290.9(64)	"	"	34.547	97.15	-0.00598	-0.03546 (1.6)	-0.08033 (2.9)	-0.1444 (0.97)	-0.2261 (1.9)	-0.3326		P	0°P.P., Power Shutdown-Arc
7	12-13-1501	"	2.80E-3(2.1E-6)	288.2(59)	"	"	95.502	268.56	+0.01396	+0.05385 (11)	+0.1415 (2.0)	+0.2751	+0.4765	+0.6380		B	boundary- 90°P.P.
8	1-2-1450	"	1.20E-3(9.0E-6)	288.2(59)	"	"	97.383	273.85	+0.01914	+0.07576	+0.1764 (0.81)	+0.3321	+0.5482			B	90°P.P., Al Foil on Wall Ports
9	1-9-1318	"	7.60E-3(5.7E-5)	288.2(59)	"	"	95.496	268.54	+0.1006	+0.2723						B	90°P.P., Al Foil on Feedthrough
10	1-9-1358	"	7.60E-3(5.7E-5)	288.2(59)	"	"	95.449	274.03	+0.03086	+0.1311 (0.62)	+0.3036 (0.06)	+0.5620	+0.9216			B	90°P.P., Repeat of Test 9
11	1-11-0904	"	6.67E-3(5.0E-5)	288.2(59)	"	"	36.094	101.50	-0.01045	-0.04294 (3.0)	-0.09776 (1.4)	-0.1754	-0.2778			P	0°P.P.
12	1-11-1337	"	6.27E-3(4.7E-5)	288.2(59)	"		36.079	101.46	-0.00295	-0.03484 (27)	-0.08250 (18)	-0.1691	-0.2657			P	0°P.P., Ion Gauge Off
13	1-16-1301	"	8.00E-3(6.0E-5)	288.7(60)	"		35.158	98.87	-0.00861	-0.03931 (0.00)	-0.08659 (8.6)					P	0°P.P., Al Foil on All Parts
14	1-17-__	"	~8.00E-3(6E-5)	~288.2(59)	G(P)	- B	88.231	248.11	+0.01754	-0.07376 (0.36)	+0.1643					B	90°P.P.

Table 5. Boundary Effects Test Summary

Test No.	Date-Time Mo-Da-Hour (1989-1990)	Device No.	Pressure Pa(torr)	Temp. °K(°F)	Voltage Polarities: Top (B=ball, P=plate)	Voltage Polarities: Bottom (B=ball, P=plate)	Equilibrium: Position x_0(in)	Equilibrium: Angle($\Delta 2$) θ(deg)	Total Force - μ N ($\pm$ 1σ, %): Voltage Between Electrodes, kV: 5	10	15	20	25	30	33	Force Toward (B=ball, P=plate) [See Note 1]	Remarks
15	1-17-__	1A	~8.00E-3(6E-5)	~288.2(59)	G(P)	+B	96.65	271.78	+0.04186 (6.7)	+0.1894 (1.8)						B	90°P.P.
16	1-18-__	"	~8.00E-3(6E-5)	~288.2(59)	"	"	96.54	271.47	+0.04745	+0.1982	+0.4745					B	90°P.P.
17	1-18-__	"	~8.00E-3(6E-5)	~288.2(59)	"	"	96.53	271.46	+0.00339 (108)	+0.02212 (1.2)	+0.07132 (0.82)					B	90°P.P., Plate 1-in from Wall
18	2-14-__	"	~8.00E-3(5E-5)	~288.2(59)	+ $\frac{V}{2}$ (B)	- $\frac{V}{2}$ (P)											0°P.P., Bkdn Over Glass Rod
19	2-19-__	"	~8.00E-3(6E-5)	~288.2(59)	"	"											0°P.P., Acrylic Replace Glass Rod, Bkdn again
20	3-15-1515	"	~8.00E-3(6E-5)	~288.2(59)	"	"	38.694	108.81	-0.00558	-0.02113 (19)	-0.05024 (2.3)	-0.1013				P	0°P.P., Glass Disk Insulation
21	3-19-1345	"	1.03E-3(7.7E-6)	290.9(64)	"	"	98.889	278.08	+0.005577	+0.02231 (0.22)	+0.05896 (1.9)	+0.1028	+0.1498			B	90°P.P.
22	3-19-1608	"	9.87E-4(7.4E-6)	290.9(64)	- $\frac{V}{2}$ (B)	+ $\frac{V}{2}$ (P)	98.950	278.25		+0.03781 (5.3)						B	90°P.P., Reverse Polarity
23	3-20-1350	"	5.87E-4(4.4E-6)	288.7(60)	+ $\frac{V}{2}$ (B)	- $\frac{V}{2}$ (P)	98.968	278.30		+0.02312	+0.06458	+0.1108				B	90°P.P., No Mass or Light Effects
24	3-20-__		~6.67E-4(5E-6)	~288.7(60)	- $\frac{V}{2}$ (B)	+ $\frac{V}{2}$ (P)											90°P.P., Reversed Polarity
25	3-22-1336	2A	2.40E-3(1.8E-5)	290.9(64)	"	"	92.891	261.22	-0.004302	-0.04693						P	0°P.P., Use Acrylic in Test Device
26	3-22-1502		1.60E-3(1.2E-5)	290.9(64)	"	"											0°P.P., Small V Steps, Noisy Data
27	NO TEST																
28	3-26-1330	2A	3.33E-4(2.5E-6)	292.6(67)	G(P)	+B	40.556	114.05		-0.00864 (94)		-0.05717 (5.9)	-0.06516 (4.4)	-0.1230 (3.1)	-0.1342	P	0°P.P., Bkdn at 35kv

Table 5. Boundary Effects Test Summary

Test No.	Date-Time Mo-Da Hour (1939-1980)	Device No.	Pressure Pa(torr)	Temp. °K(°F)	Voltage Polarities: Top (B=ball, P=plate)	Voltage Polarities: Bottom (B=ball, P=plate)	Equilibrium: Position x_0(in)	Equilibrium: Angle(±2) θ(deg)	Total Force - μ N (± 1σ, %): Voltage Between Electrodes, kV: 5	10	15	20	25	30	35	Force Toward (B=ball, P=plate) [See Note 1]	Remarks
29	3-26-1455	2A	3.33E-4(2.5E-6)	292.6(67)	G(P)	-B											0°P.P., Blade Problems, Poor Data
30	3-30-0900	"	1.33E-4(1.0E-6)	290.4(63)	"	-B	111.305	313.00		+0.05073		+0.1361	+0.2735	+0.4445		B	90°P.P., Questionable Data, Blade at 35kv
31	3-30-0945	"	1.33E-4(1.0E-6)	290.9(64)	"	+B	111.384	313.16		+0.04536		+0.1799	+0.2738	+0.3793		E	90°P.P., Blade at 35kv

NOTE 1: The sign of the measured force in tests 1 through 31 have been made self-consistent, even though the measuring scales used for tests 1-17 differed from the scales used for 18-31. The device orientation was reversed for all tests after No. 31.

shakedown of the new torsion pendulum system and the power supplies. Drift of the equilibrium position of the pendulum was found to be non-zero, but was generally steady and rather small, and was, therefore, readily correctable. In Test No. 2, for example, the zero drift was significant, was about 0.00114 in per swing of the pendulum, and was consistent over 50 swings (about 22 min) during the test run. For these tests, the measured forces were small, and varied approximately as the second power of the driving voltage between electrodes of the test devices.

Test No. 7 was conducted using a zero equilibrium position shifted by about 90 degrees with respect to that used for the first six tests. The indicated angular position θ corresponded to the observed position x_0 on the tank mounted scale, as seen in the second mirror (shifted by about 90° with respect to the first mirror). The exact values of the position x_0 and angle θ shown in Table 5, were determined from corrections obtained by reading a single scale using both mirrors, and by reading two scales using a single mirror.

In Tests 8 through 10, successive amounts of aluminum foil shielding were added over various chamber ports and feed throughs. Test No. 9 results should be disregarded as a computer shutdown of power was experienced, together with a large zero shift in pendulum equilibrium position.

Test Nos. 7 through 10 gave the first indications that some type of boundary effects were significant, in that the direction of the forces for these tests (with a 90° shift in zero equilibrium position) was reversed from the direction obtained when the equilibrium position of the pendulum was near zero degrees.

To confirm that this was the case, and the shift in force direction was not due to effects arising from application of the

aluminum foil shielding, or from some residual ion generation from the ion vacuum gauge, Test Nos. 11, 12, and 13 were run. These tests confirmed the reversal in direction of the apparent force with change in pendulum equilibrium position. The corresponding forces for these tests were in better agreement with each other, even though their magnitude was not the same as observed in Test Nos. 7 through 10.

In further search of possible boundary effects, Test Nos. 14 through 16 were run, again near the 90° pendulum position, but with the top fiber grounded, so the electrical potential to the test device was applied through the bottom fiber. This choice was in response to the belief that some residual boundary effect was arising from the inability to properly shield the off-center electrical feedthrough at the top of the chamber. With the top fiber grounded, such an effect should have disappeared; but it did not.

Test No. 17 was conducted in the same 90° pendulum position, with the grounded boundary plate moved inward 2.5 cm (1.0 in) from the tank wall toward the pendulum. The corresponding variation of the apparent force with applied voltage, V, changed from approximately a V^2 dependence to one of about $V^{2.7}$. This further indicated that boundary effects could significantly alter the measured force.

Additional possible sources of boundary effects were the corona shields emplaced in early tests around the upper and lower fibers of the dual torsion fiber force measurement system. Careful examination revealed that the torsion fibers were not accurately coaxial with the cylindrical corona shields. Since the prospect of achieving and maintaining the precision fiber-tube alignment presumably required was not attractive, a better choice was to remove the corona shields. The original purpose of the shields was to minimize corona discharge over the vacuum

range from atmospheric pressure down to about 1.33 Pa (1.0×10^{-2} torr). At the lower gas pressure of 1.33×10^{-2} Pa (1.0×10^{-4} torr) to 1.33×10^{-4} Pa (1.0×10^{-6} torr) of interest here, the need for the corona shields was far less significant. Therefore, the shields were removed.

Beginning with Test No. 18, preparations were made to enable deflections of the torsion pendulum to be evaluated over a full 180° range of equilibrium positions. With the tandem mounting arrangement of two test devices on the device holder, this would correspond to a complete period of equilibrium positions in azimuth for symmetric configuration. This approach would permit force measures to be made in the presence of residual boundary effects, and the average of the measured force values over the 180° range of equilibrium positions should represent the electrostatically generated steady force (if any) on the test devices. The measured values of the apparent force would, therefore, represent the sum of the boundary induced force and the average or steady force.

In implementing this approach, additional Test Nos. 18 through 20 were conducted to overcome surface electrical breakdown problems over the insulators separating the upper and lower elements of the device support system.

Test No. 21 again showed a reversal in direction of apparent force with shift in pendulum equilibrium position.

Test No. 22 indicated no such shift in direction occurred merely with a reversal in polarity of voltage driving the test device (compared to Test No. 21).

In Test No. 23 possible effects of incident light on the test device were shown to be negative. Further, an additional mass of 45 kg (100 lb) placed against the outside of the vacuum

chamber did not cause any observable perturbation in the apparent force measured.

No data was obtained from Test No. 24 as an apparent electrical breakdown across the test devices caused the high voltage power sources to shutdown.

In Test Nos. 25 through 31, test devices of type No. 2A with a dielectric rod of acrylic between the electrodes were used. The data for Test Nos. 25, 26, 29 and 30 were poor or questionable due to further breakdown problems. The results for Test Nos. 28 and 31 appear to be reasonable at the pendulum equilibrium positions of 0° and 90°, respectively. In each of these two cases the apparent forces varied approximately as the square of the applied voltage. Further, there seemed to be no significant variation from this functional dependence at the larger applied voltages. Finally, the directions of the apparent forces observed at 0° and 90° equilibrium positions seemed consistent during these last tests, and throughout all the tests indicated in Table 5.

It was concluded from Test Nos. 1 through 31 that boundary effects were significant. Also these results implied that the force generation tests should be run at several angles over a 180° range of zero equilibrium positions of oscillation of the torsion pendulum in order to determine the presence (or absence) of an average non-zero force which might be attributed to the Biefield-Brown effect. Finally, these tests also indicated that during each experimental run, the individual voltages applied to the devices should be repeated several times to enable statistical estimates to be made for each corresponding force level obtained.

Device Tests

The propulsion device tests conducted under this program followed the approach just noted. Three major changes were made from the previous boundary effects tests.

- Due to significant shielding problems of the high voltage feed through and leads at the top of the chamber, the upper fiber was connected through the electrometer to the same earth ground as the chamber walls. While this caused an electrical asymmetry to be present in the chamber, this was not expected to create an abnormal situation which would cause a steady torque to appear on the test device and be interpreted as a propulsive force.

- The orientation of the asymmetrical devices used in Test Nos. 32 and higher were reversed from that used in Test Nos. 1 through 31. This, coupled with the preceding change, enabled the electrical hookup to the asymmetrical test devices to be the same as was used in the Phase I program.[1] In both cases, the ball electrode (in a ball and plate type device) was at or very near the same earth ground as the chamber walls. Changes in the electrical polarity of potentials applied to the test devices were made via the bottom fiber. Due to the reversal in device direction, the sign associated with the apparent forces in Test Nos. 32 and higher was reversed from that in Test Nos. 1 through 31. The positive force direction in Test No. 32, for example, corresponded to a force directed from the ball toward the plate; this positive direction also corresponded to the positive x direction of deflection of the center of oscillation of the pendulum.

- The electrode separation in the test devices was shortened to increase the electric field strength within the device for the same applied voltage. For the asymmetrical ball and plate device the on-axis electrode separation was decreased from 0.0483 m (1.90 in) to 0.0190 m (0.750 in), and the corresponding field strength was increased by a factor of about 2.5 for the same applied voltage.

The test conditions and resulting forces measured using the several test devices (except Nos. 1A and 2A) specified in Table 2, are given in Table 6. Each tabular entry of the total force represents an average value obtained in either three or four repetitions of the individual voltage steps applied to the test devices. Approximately seven to ten force measures were obtained per voltage step from deflections of the center of oscillation for each swing of the torsion pendulum. In parenthesis following each average force entry is an unbiased estimate of the associated standard deviation, expressed as a percentage of the average force, and obtained from the experimental data.[7]

In all cases the force measures within a voltage step were far more precise than their repeatability from step-to-step, so the standard deviation applies principally to the repeatability of forces among steps within a given test run. In a few instances, repetition of the voltage steps was not obtained, and only one set of force measurements (within a single step) was obtained. For these cases, no statistical estimates of variations among the steps were possible; these are denoted in Table 6 by a dash within parenthesis, (-), following each such force value.

The average force values for Test Device No. 2B observed in each of the Test Nos. 32, 33, and 36 to 47 given in Table 6 are

Table 6. Devices Test Data Summary

Test No.	Date-Time Mo-Da-Hour (1990)	Device No.	Pressure Pa(torr)	Temp. °K(°F)	Voltage Polarities		Equilibrium		Total Force - μ N (± 1σ, %)				Remarks
					Top (B=ball, P=plate)	Bottom (B=ball, P=plate)	Position x_0(in)	Angle(x2) θ(deg)	Voltage Between Electrodes, kV				
									5	10	15	19	
32	4-12-0903	2B	2.27E-4(1.7E-6)	291.5(65)	G(B)	+(P)	41.912	117.86	+0.02230(3.6)	+0.06392(14.4)	+0.1458(0.89)	–	
33	4-12-1335	2B	2.13E-4(1.6E-6)	292.6(67)	G(B)	-(P)	41.872	117.75	+0.01805(6.7)	+0.06111(2.5)	+0.1385(2.2)	+0.2293(1.9)	
34	4-16-1400	2B	1.50E-4(1.2E-6)	292.0(66)	G(B)	-(P)	41.586	116.94	+0.04938(-)	+0.1479 -	+0.3371(-)	–	w/ Bndry Plate in 0.5 in from wall Device Bounced; Aborted Test
35	4-17-1430	2B	1.47E-4(1.1E-6)	290.9(64)	G(B)	-(P)	41.191	115.82	+0.04641(15)	+0.1399(7.0)	+0.3118(3.5)	+0.5079(-)	Repeat of No. 34
36	4-19-0915	2B	1.33E-4(1.0E-6)	292.6(67)	G(B)	-(P)	53.199	149.60	+0.02640(7.0)	+0.08196(4.8)	+0.1986(0.59)	+0.3236(.92)	
37	4-19-1310	2B	1.33E-4(1.0E-6)	292.6(67)	G(B)	+(P)	53.142	149.44	+0.02938(-)	+0.09156(3.6)	+0.2027(3.8)	+0.3234(-)	
38	4-23-1300	2B	1.33E-4(1.0E-6)	292.0(66)	G(B)	-(P)							Aborted Test, Power Shutdown
39	4-24-0951	2B	1.16E-4(8.7E-7)	292.0(66)	G(B)	-(P)	87.540	246.17	+0.00385(20)	+0.01200(14)	+0.03180(24)	+0.04874(4.2)	
40	5-3-1300	2B	4.93E-4(3.7E-6)	294.8(71)	G(B)	-(P)							Aborted Test, Procedure Error
41	5-3-1505	2B	5.06E-4(3.8E-6)	294.8(71)	G(B)	-(P)	71.636	201.44	+0.01660(13)	+0.06834(1.5)	+0.1551(0.11)	+0.2503(0.50)	
42	5-4-0911	2B	3.73E-4(2.8E-6)	294.3(70)	G(B)	+(P)	71.581	201.29	+0.01918(0.58)	+0.07338(1.5)	+0.1639(0.96)	+0.2541(1.9)	
43	5-7-1340	2B	2.40E-4(1.8E-6)	294.3(70)	G(B)	-(P)	95.632	268.92	-0.01027(18)	-0.03003(15)	-0.07022(12)	-0.1063(0.92)	
44	5-8-0950	2B	2.40E-4(1.8E-6)	294.3(70)	G(B)	-(P)	119.396	335.75	-0.02752(19)	-0.1074(2.3)	-0.2432(2.6)	-0.3869(1.7)	
45	5-8-1441	2B	2.67E-4(2.0E-6)	295.4(72)	G(B)	+(P)	119.338	335.59	-0.02442(7.8)	-0.1069(1.0)	-0.2388(1.0)	-0.3843(.80)	
46	5-14-1105	2B	1.60E-4(1.2E-6)	295.4(72)	G(B)	-(P)	13.787	38.77	-0.01627(24)	-0.06627(2.2)	-0.1455(1.1)	-0.2334(1.2)	
47	5-16-1330	2B	1.60E-4(1.2E-6)	295.9(73)	G(B)	-(P)							Aborted Test, Power Shutdown
48	5-25-0930	5	3.47E-4(2.6E-6)	295.4(72)	G(B)	-(B)	60.390	169.82	+0.00960(29)	+0.04554(44)	+0.08347(1.7)	+0.1345(.66)	
49	5-25-1326	5	3.20E-4(2.4E-6)	295.4(72)	G(B)	+(B)	60.300	169.57	+0.01032(22)	+0.04152(6.2)	+0.09725(1.7)	+0.1399(0.87)	
50	5-29-1131	5	1.07E-4(8.0E-7)	296.5(74)	G(B)	-(B)	121.075	340.47	-0.01748(8.2)	-0.07535(3.6)	-0.1727(0.66)	-0.2790(0.35)	Possible Pendulum Zero Shift
51	6-4-1141	5	8.00E-5(6.0E-7)	296.5(74)	G(B)	-(B)	82.397	232.27	-0.00827(-)	-0.01507(51)	0.02322(10)	-0.03412(4.8)	Very Small Force, Data Questionable

Table 6. Devices Test Data Summary

Test No.	Date-Time (Mo-Da-Hour, 1990)	Device No.	Pressure Pa(Torr)	Temp. °K(°F)	Voltage Polarities: Top (B=ball, P=plate)	Voltage Polarities: Bottom (B=ball, P=plate)	Equilibrium: Position x_0(in)	Equilibrium: Angle(x2) ϕ(deg)	Total Force - μ N ($\pm$ 1σ, %): Voltage Between Electrodes, kV: 5	10	15	19	Remarks
52	6-6-1131	5	7.20E-4(5.4E-7)	297.0(75)	G(B)	-(B)	51.501	144.82	+0.01105(44)	+0.04154(2.9)	+0.09469(4.2)	+0.1541(2.2)	
53	6-12-1420	6	2.67E-3(2.0E-5)	297.0(75)	G(P)	-(P)	57.281	161.08	+0.01437(26)	+0.05904(2.3)	+0.1346(0.70)	+0.2175(1.2)	
54	6-18-0957	6	3.07E-4(2.3E-6)	297.6(76)	G(P)	-(P)	50.095	142.96	+0.01626(26)	+0.07936(5.0)	+0.17..0(3.0)	+0.2840(0.83)	
55	6-19-1000	6	1.33E-3(1.0E-5)	292.7(70)	G(P)	-(P)	119.323	336.54	-0.01793(8.2)	-0.07983(1.5)	-0.181.(0.89)	-0.2890(0.61)	
56	6-19-1500	6	1.04E-3(7.8E-6)	298.2(77)	G(P)	+(P)							Pulsed Power Test; No Motion HZ: 0, 10, 60, 180, 400, 600
57	6-20-0844	6	4.40E-4(3.3E-6)	298.2(77)	G(P)	-(P)	109.864	308.92	-0.01442(4.5)	-0.06669(1.7)	-0.1550(0.52)	-0.2521(0.29)	
58	6-22-0920	6	1.60E-4(1.2E-6)	297.8(76)	G(P)	-(P)	55.321	155.57	+0.01612(14)	+0.07350(1.5)	+0.1716(0.46)	+0.2772(0.27)	
59	6-22-1510	6	1.73E-4(1.3E-6)	296.7(78)	G(P)	+(P)							Pulsed Power Test, No Motion HZ: 0, 10, 60, 180, 400, 600
60	6-25-0908	6	1.33E-4(1.0E-6)	296.5(74)	G(P)	+P	59.761	168.05	+0.01573(14)	+0.06778(2.8)	+0.1546(0.93)	+0.2518(0.37)	
61	6-27-1315	1B	6.40E-4(4.8E-6)	297.8(76)	G(B)	-P	59.230	166.56	--	+0.08036(11)	+0.2117(1.8)	+0.3331(1.8)	
62	6-27-1545	1B	5.07E-4(3.8E-6)	297.6(76)	G(B)	+P			--				Pulsed Power Test, No Motion HZ: 0, 10, 60, 180, 400, 600
63	6-29-1015	1B	2.13E-4(1.6E-6)	297.6(76)	G(B)	-P	124.800	350.95	--	-0.07453(0.4)	-0.1784(5.4)	-0.2813(0.36)	Pendulum Zero Shift. Data Questionable
64	6-29-1410	1B	1.87E-4(1.4E-6)	298.2(77)	G(B)	-P	125.413	352.67	--	-0.07722(3.3)	-0.1817(2.2)	-0.2934(1.3)	Further Pendulum Zero Shift. Data Questionable
65	7-2-1140	1B	2.93E-4(2.2E-6)	297.0(75)	G(B)	-P	125.314	352.39	--	-0.08391(2.6)	-0.1908(1.5)	-0.3081(0.39)	Pendulum Zero Shift, Data Questionable
66	7-3-1000	1B	1.33E-4(1.0E-6)	297.0(75)	G(B)	-P							Aborted Test. Pendulum Zero Shift
67	7-6-1347	1B	1.47E-4(1.1E-6)	297.6(76)	G(B)	-P	125.033	351.60	--	-0.08095(0.57)	-0.2048(0.33)	-0.3277(0.71)	
68	7-10-1300	1B	6.27E-5(4.7E-7)	299.3(79)	G(B)	-P							Pulsed Power Test, Modified Supply; Aborted Test Due to Supply Failure

Table 6. Devices Test Data Summary

Test No.	Date-Time Mo-Da-Hour (1990)	Device No.	Pressure Pa(torr)	Temp. °K(°F)	Voltage Polarities		Equilibrium		Total Force - μ N (± 1σ, %)				Remarks
					Top (B=ball, P=plate)	Bottom (B=ball, P=plate)	Position z_0(in)	Angle(x2) θ(deg)	Voltage Between Electrodes, kV				
									5	10	15	19	
69	7-12-1045	1B	9.33E-5(7.0E-7)	298.2(77)	G(B)	-P	124.902	351.23					Repeat of Test 68; At 19kV, Max Force Less than 2% of Result in Test 67
70	7-18-1113	6	7.33E-5(5.5E-7)	299.8(80)	G(P)	-P	120.748	339.55	–	-0.08210(0.92)	-0.1874(0.40)	-0.3004(0.09)	
71	7-18-1300	6	7.73E-5(5.8E-7)	299.8(80)	G(P)	+P	120.745	339.54	–	-0.08492(1.9)	-0.1900(0.65)	-0.3062(0.64)	
72	7-19-1008	4	1.87E-4(1.4E-6)	299.8(80)	G(B)	-B	121.767	342.42	-	-0.05682(0.75)	-0.1287(0.81)	-0.2070(0.93)	
73	7-19-1300	4	1.60E-4(1.2E-6)	300.4(81)	G(B)	+B	121.868	342.70	–	-0.05675(3.5)	-0.1281(0.46)	-0.2053(0.36)	
74	7-20-1414	4	1.09E-4(8.2E-7)	300.4(81)	G(B)	-B	55.423	155.85	–	+0.05075(2.6)	+0.1173(0.74)	+0.1879(0.53)	
75	7-23-0916	4	8.13E-5(6.1E-7)	298.2(77)	G(B)	-B	53.367	150.07	–	+0.05043(0.96)	+0.1171(1.6)	+0.1884(0.34)	Aborted Test; Computer Failure
76	7-25-1617	5	7.73E-4(5.8E-6)	299.8(80)	G(B)	-B							
77	7-26-1013	5	2.27E-4(1.7E-6)	298.7(73)	G(B)	-B	53.836	151.39	–	+0.04255(4.5)	+0.09520(1.7)	-0.1501(1.0)	
78	7-26-1145	5	2.27E-4(1.7E-6)	299.3(79)	G(B)	+B	53.989	151.82	–	+0.04541(12)	+0.1016(3.3)	+0.1616(1.9)	
79	7-27-1020	5	4.67E-4(3.5E-6)	299.3(79)	G(B)	-B	120.915	340.02	–	-0.05139(1.9)	-0.1104(2.2)	-0.1802(0.62)	
80	7-27-1120	5	4.40E-4(3.3E-6)	299.8(80)	G(B)	+B	119.447	335.89	–	-0.01828(7.4)	-0.07597(1.2)	-0.1538(0.60)	
81	8-1-1110	2C	7.87E-3(5.9E-5)	298.7(78)	G(B)	-P							Anomalous (See Text)
82	8-2-0852	2C	1.33E-3(1.0E-5)	298.7(78)	G(B)	-P							Anomalous (See Text)
83	8-2-1447	2C	1.33E-3(1.0E-5)	299.8(80)	G(B)	-P							Aborted Test; Voltage Fluctuations
84	8-3-1606	3	~1.33E-3(1.0E-5)	298.7(78)	G(B)	-P	122.311	343.64	–	-0.08211(2.7)	-0.1959(2.0)	-0.2936(1.4)	
85	8-9-0904	3	~1.33E-3(1.0E-5)	297.6(76)	G(B)	+P	122.203	343.64	–	-0.08543(1.7)	-0.1909(.89)	-0.3018(1.0)	
86	8-10-0906	3	~1.33E-3(1.0E-5)	298.7(78)	G(B)	-P	61.007	171.55	–	+0.08107(2.7)	+0.1635(.62)	+0.2997(3.6)	
87	8-10-1045	3	~1.33E-3(1.0E-5)	299.3(79)	G(B)	+P	61.005	171.55	–	+0.08015(13)	+0.1891(1.6)	+0.3002(0.91)	

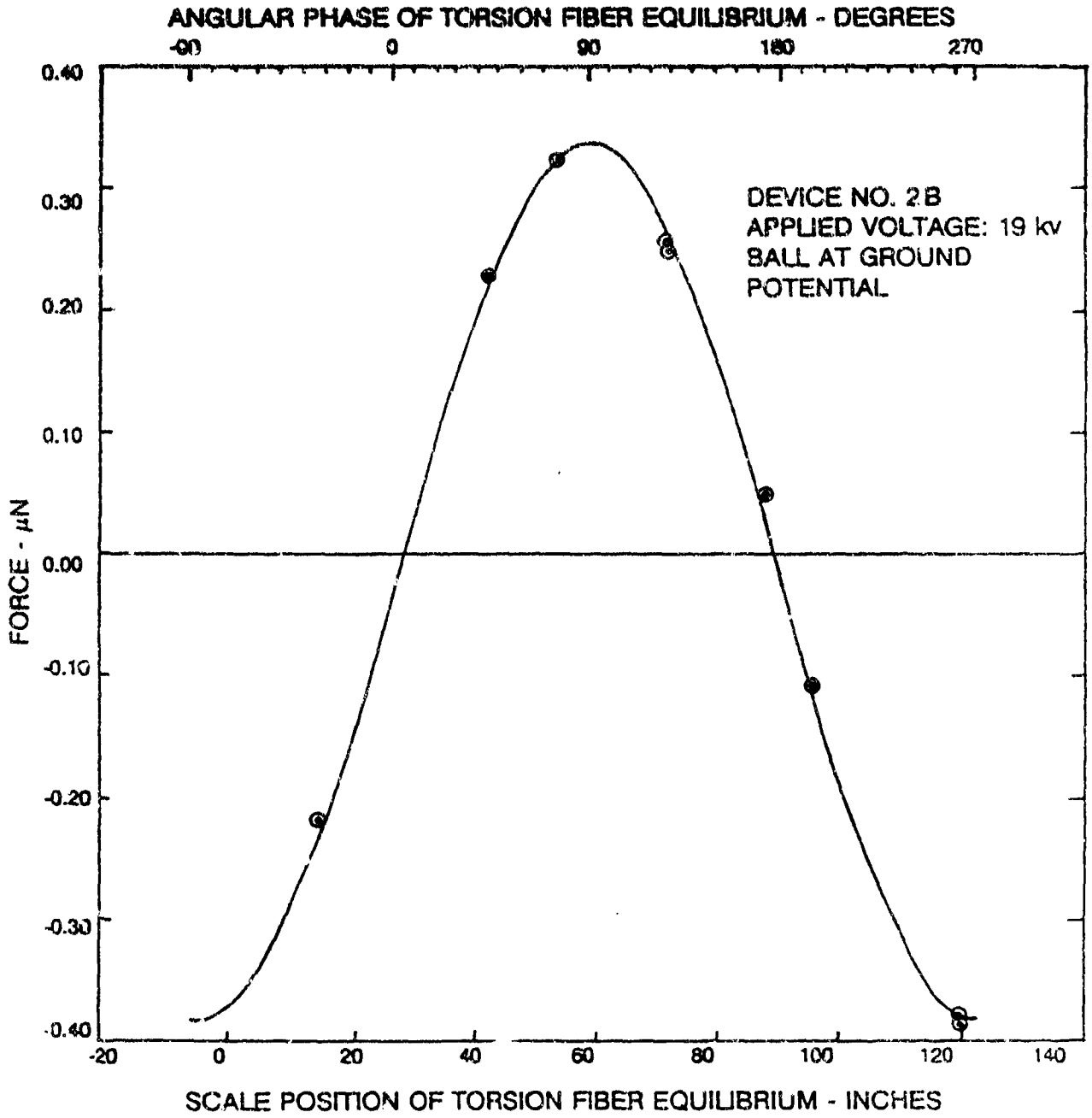

Figure 11. Variation of Measured Total Force with Angular Position of Torsion Fiber Equilibrium for Test Device No. 2B

plotted in Figure 11 as a function of the scale positions of equilibrium of the torsion pendulum. When the apparent equilibrium position was changed from test to test, it was found that the measured forces induced by identical electrical driving potentials varied periodically with an actual angular period of 180 degrees, and an apparent angular period of 360 degrees as shown in Figure 11. This periodicity, if any, was expected since the pendulum was configured with two test devices mounted in tandem and 180 degrees (actual angles) apart.

The curve drawn through the data points (i.e., total apparent force measures) represents a least squares fit of the simple periodic function

$$F = a + b\sin(\theta-\alpha), \qquad (14)$$

where α is a phase angle, and the quantity $(\theta-\alpha)$ is referred to as "angular phase of the torsion fiber equilibrium" in Figure 11 and subsequent figures.

The use of a sine function to represent the angular variation of the observed force may only be approximate, but appeared to be adequate, and useful in this program. The curve in Figure 11 is symmetric with respect to a negative, constant force value, which lies somewhat below the zero force horizontal line shown. This offset from zero indicates a non-zero value for the parameter "a" in the force representation given by Equation (14). In turn, this implies the existence of a steady torque component which acted in the same direction over the complete test. Presumably, this steady torque component could arise from the steady force of the Biefield-Brown type, so it is of potential interest here. More will be said later about this steady torque component.

Once this apparent periodicity and approximate sine function behavior was established,**** it was found more convenient to plot the force data as a function of $\sin(\theta - \alpha)$ as shown in Figure 12. The force values for 10 kV, 15 kV and 19 kV are shown in Figure 12 for Test Device 2B, but those for 5 kV were omitted because they are generally less reliable, and were not available for all of the device types tested. In the plot of Figure 12, each line through the force data points for a given drive voltage intersects the vertical axis for the angular phase $(\theta - \alpha)$ of zero, at the offset value "a." In Figure 12, this offset indicates a negative value of the steady force component "a." This corresponds to a force in the negative x direction, and for Test Device 2B from the plate toward the ball.

The steady force component "a" can be determined from two measured forces at two known θ values, or from three values of the forces and θ if α is treated as an unknown. Such a solution can also be readily obtained with additional values using least squares. The least squares approach emphasizes the force values near the maxima and minima of the sine curve. It was, therefore, convenient to utilize force measures made near these extremes, both to enhance the accuracy of the subsequent curve fits, and to reduce the number of tests required (as opposed to conducting tests over the complete 360 degree range of the angular phase). Subsequent tests were conducted with angular phases near the maximum and minimum positions.

The force measures and corresponding curves for Test Device No. 1B observed in Tests Nos. 61 and 67 are shown in Figure 13. Difficulties with pendulum zero shift, once the lower weight was in position, rendered data for several of the intervening tests

**** Further confirmation was made using data from tests with test device No. 5. Three values of α were determined and used: $\alpha = 74.82°$ for Test Device Nos. 1B, 2B and 2C and 3; $\alpha = 61.23°$ for Test Device Nos. 4 and 5; and $\alpha = 52.56°$ for Test Device No. 6.

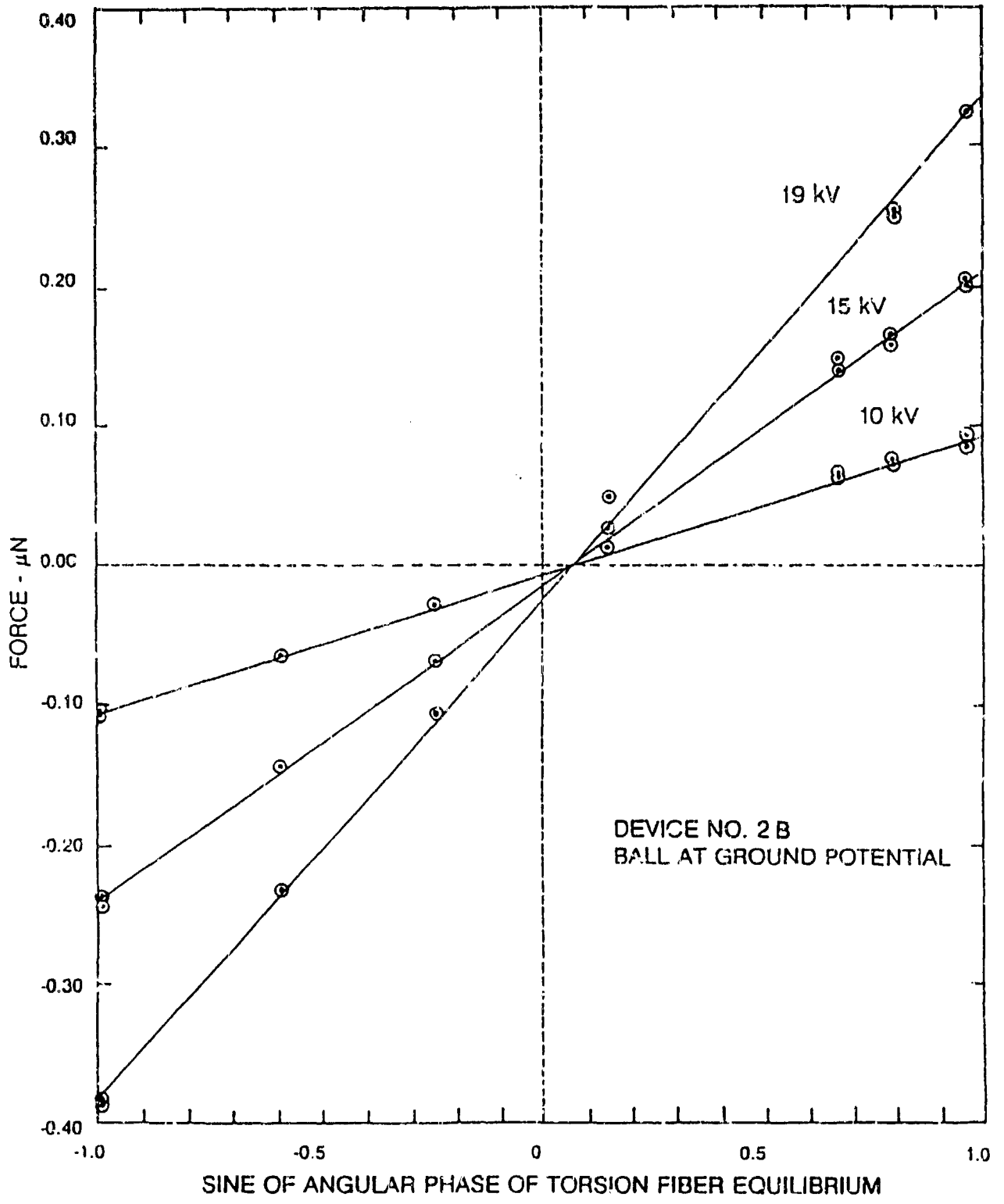

Figure 12. Variation of Measured Total Force with Angular Phase of Torsion Fiber Equilibrium for Test Device No. 2B

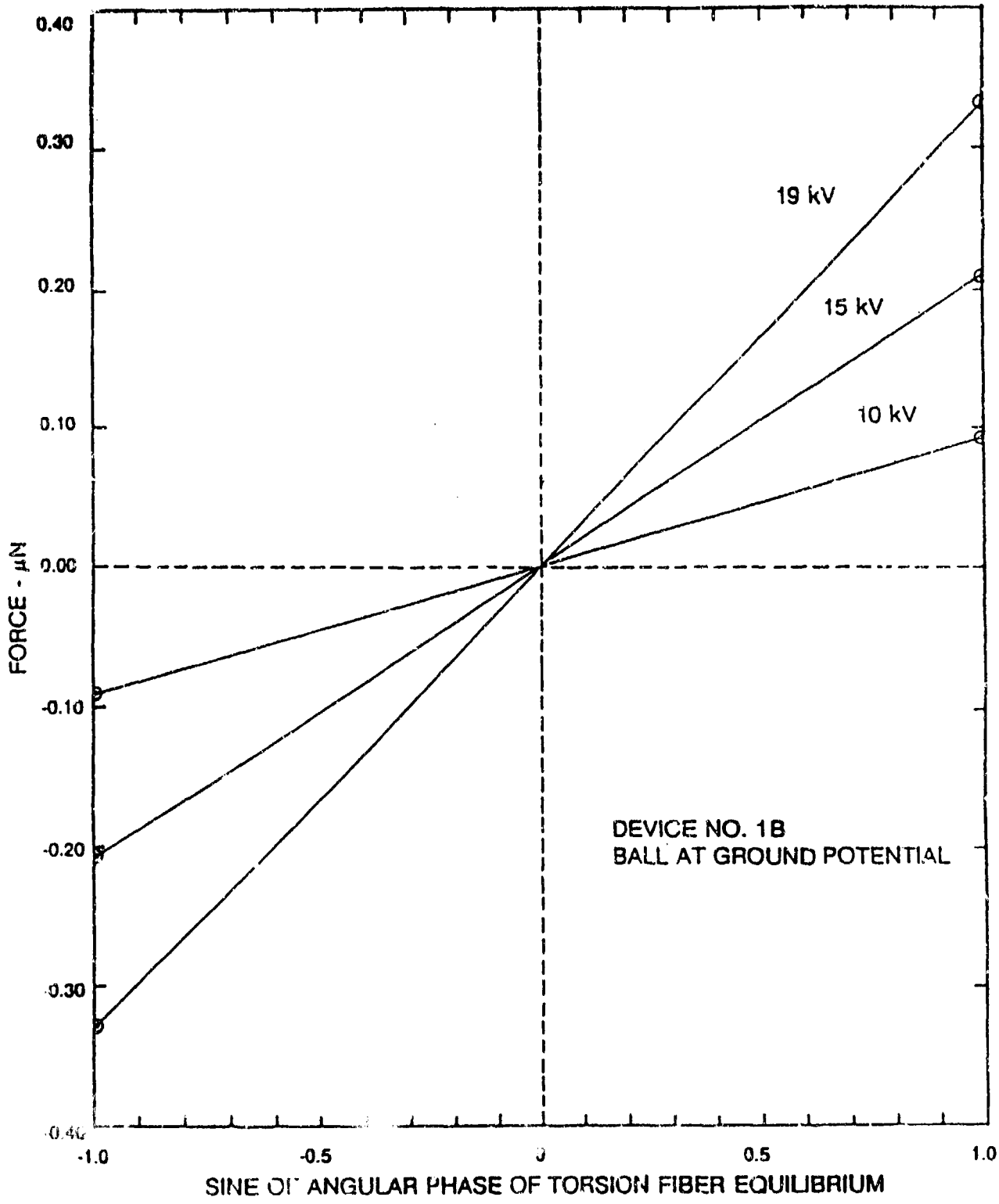

Figure 13. Variation of Measured Total Force with Angular Phase of Torsion Fiber Equilibrium for Test Device No. 1B

unreliable. No such shifts were observed during Test Nos. 61 or 67.

Similar force measures and curves for Test Device No. 3 observed in Test Nos. 84 through 87, are shown in Figure 14.

Figure 15 indicates plots of the force measures and curves for Test Device No. 4, as observed in Test Nos. 72 through 75.

Figure 16 shows plots of the forces and curves for Test Device No. 5, as observed in Test Nos. 48 through 52, and 76 through 80. There was some question about stability of the pendulum zero equilibrium in Test No. 50. The force levels were very low in Test No. 51 and the force results in this case are believed to be unreliable. Test Nos. 76 through 80 were conducted later to confirm the early results and to ensure no effects of pendulum zero shifts were present.

Figure 17 shows the force data and curves for Test Device No. 6, as observed in Test Nos. 53 through 60, and Test Nos. 70 and 71. The force levels in Test Nos. 53 and 57 appeared to be anomalous for some unknown reason (perhaps because of undetected pendulum zero shifts). Again Test Nos. 70 and 71 were conducted later to supplement the early test results.

A data summary for the steady force component values for tests shown in Figures 11 through 17 are given in Table 7, together with their associated standard deviations determined using least squares and the principle of propagation of variance.[7]

For completeness, the corresponding force amplitudes (the parameter "b" in Equation (14), for the tests and test devices of Table 7, are given in Table 8, together with their associated standard deviations.

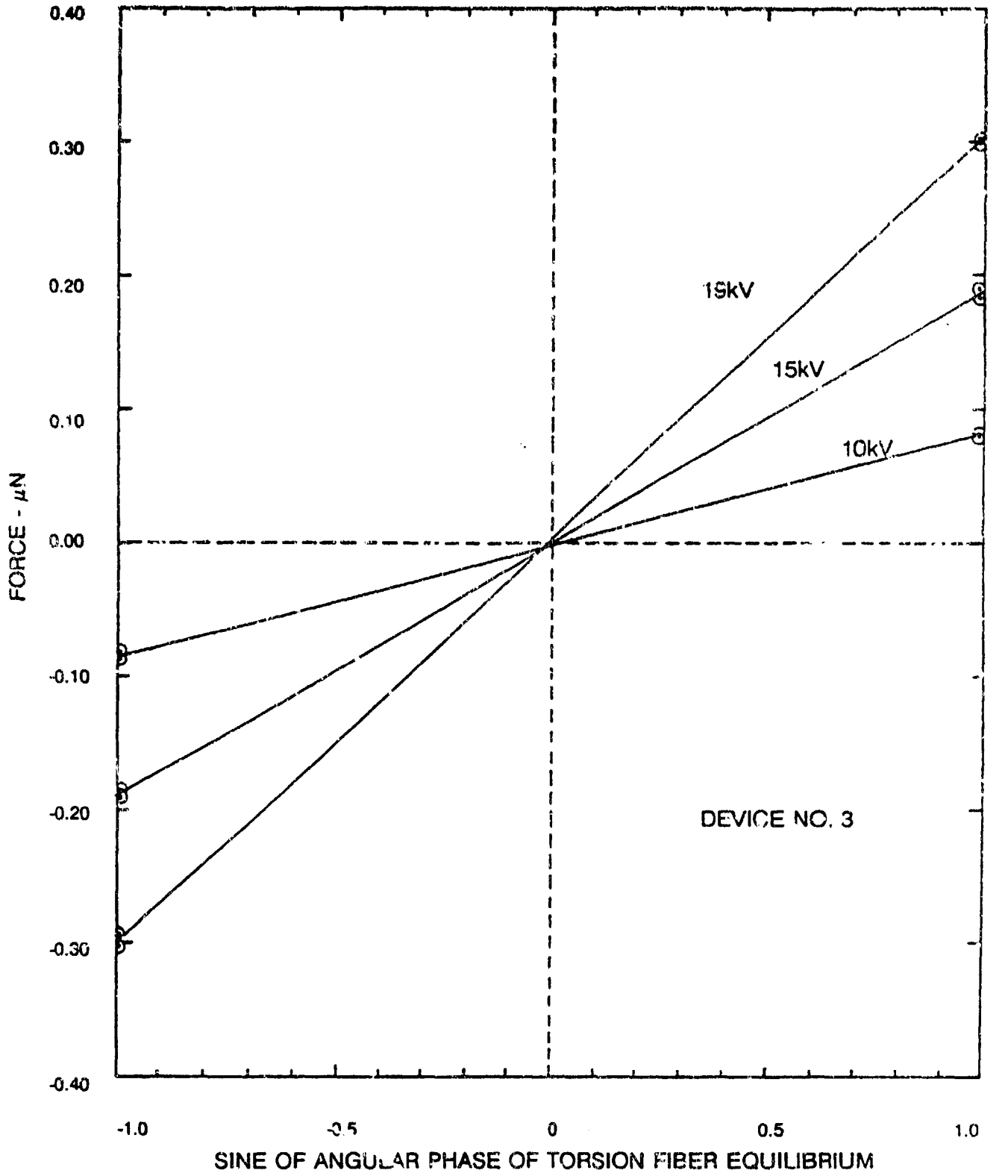

Figure 14. Variation of Measured Total Force with Angular Phase of Torsion Fiber Equilibrium For Test Device No. 3

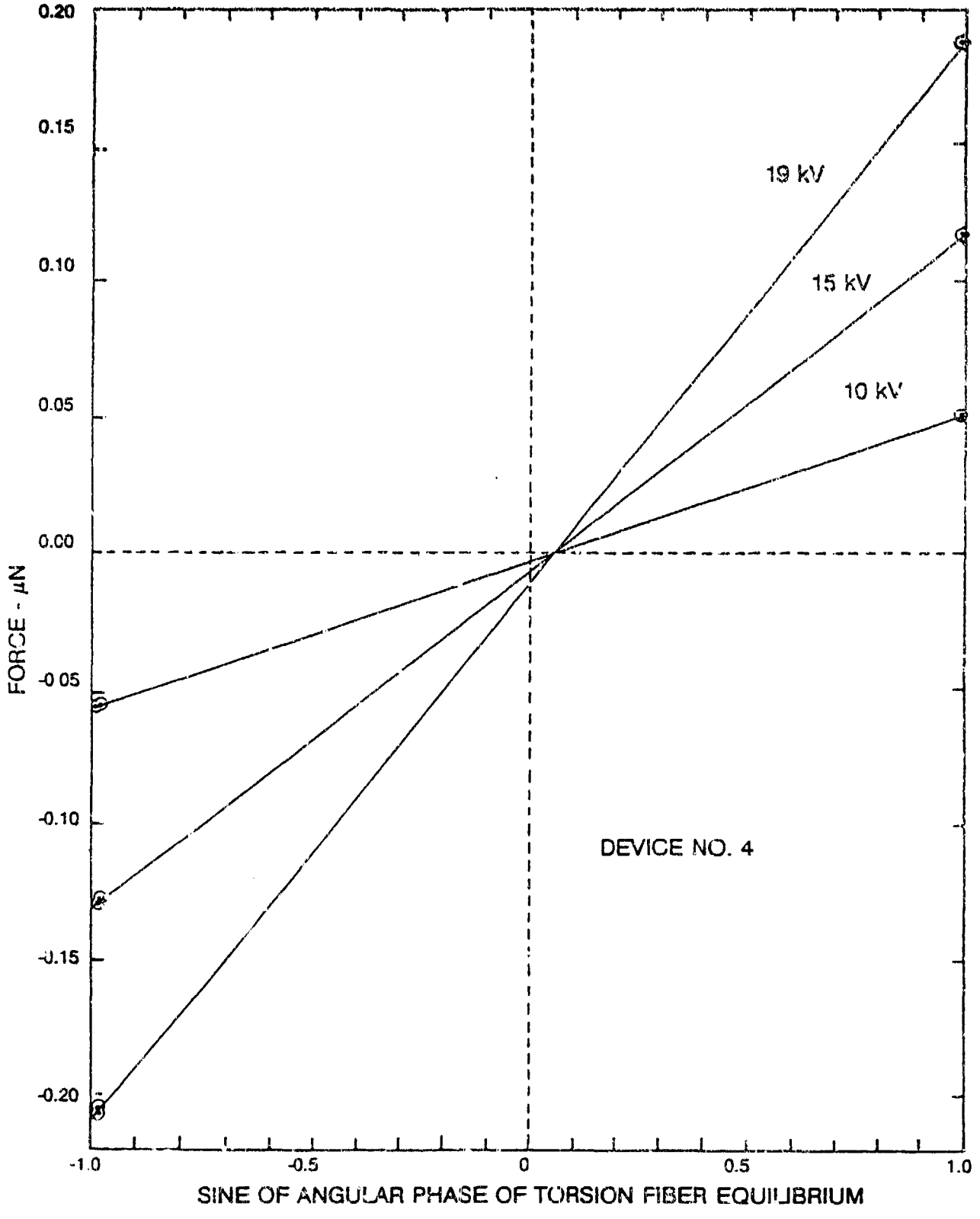

Figure 15. Variation of Measured Total Force with Angular Phase of Torsion Fiber Equilibrium for Test Device No. 4

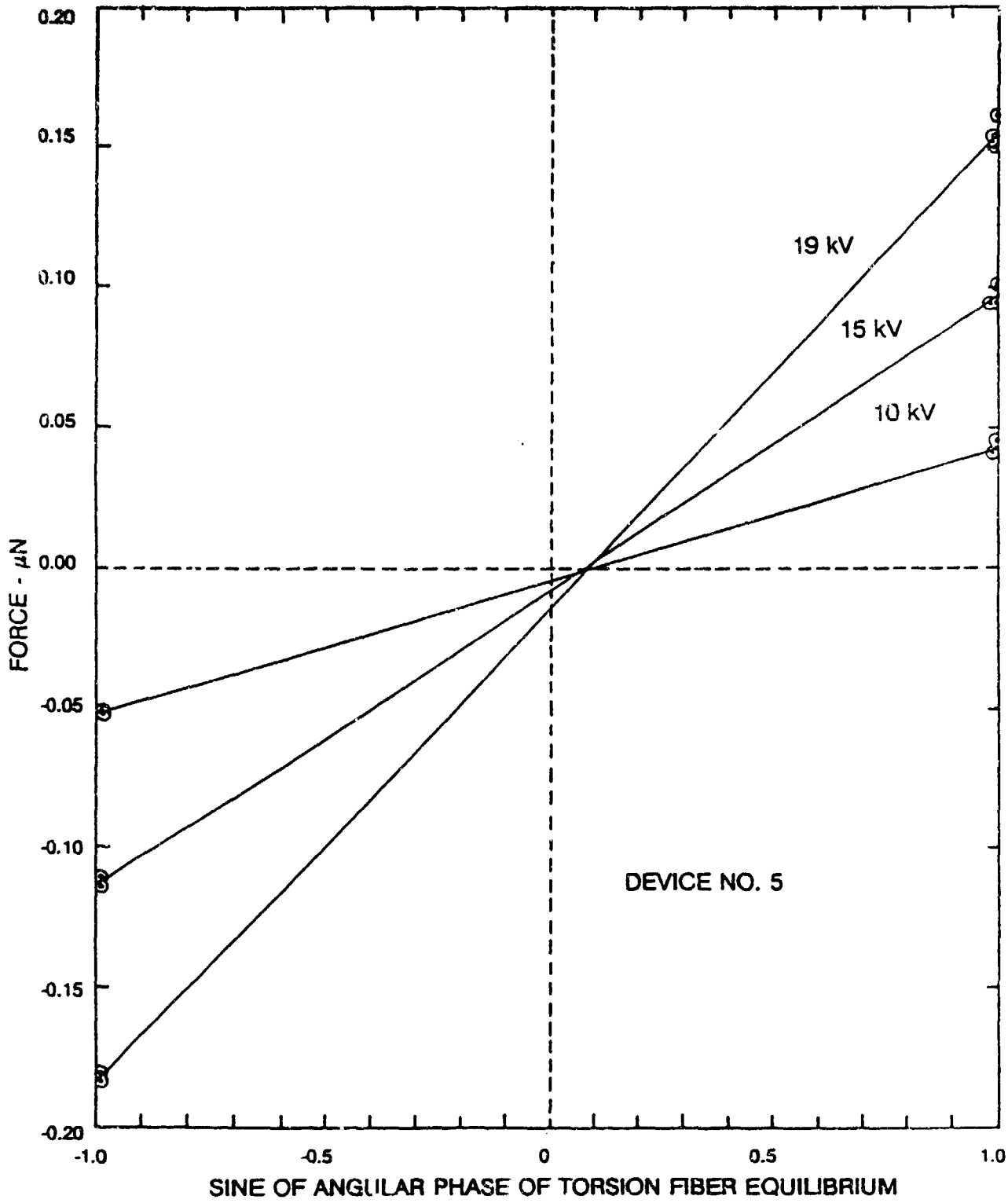

Figure 16. Variation of Measured Total Force with Angular Phase of Torsion Fiber Equilibrium for Test Device No. 5

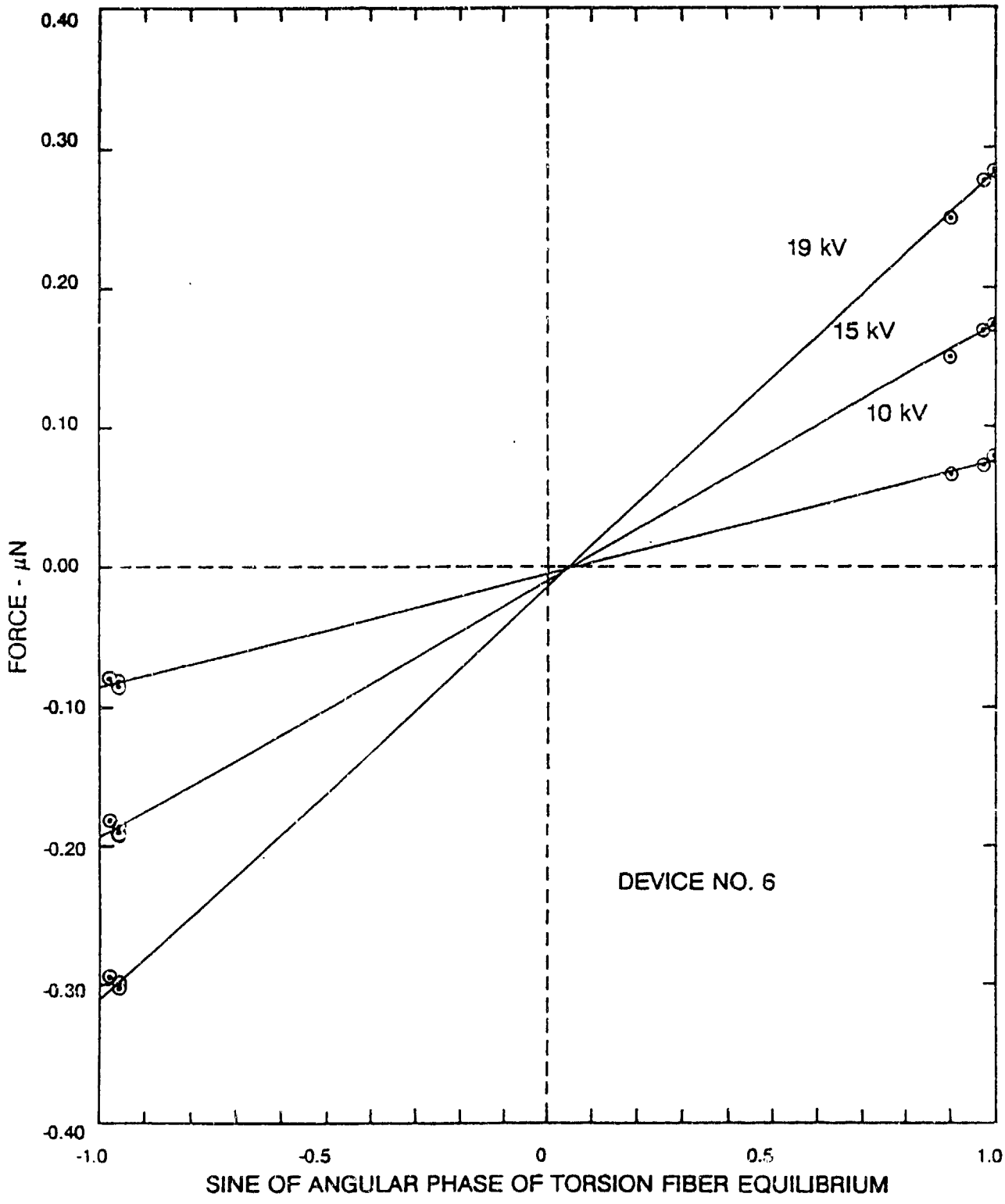

Figure 17. Variation of Measured Total Force with Angular Phase of Torsion Fiber Equilibrium for Test Device No. 6

From earlier considerations in this report, it was noted that the threshold of measurements with the torsion fiber force measuring system was about 0.64×10^{-4} m (0.0025 in). This together with the combined calibration parameter k (~ 0.0796 dyn/in) given by Equation (12), indicates the measurement threshold for residual forces is about $\pm$ 0.002 μN ($\pm$ 0.0002 dyn). This value is relevant in considering the results given in Table 7.

The results in Table 7 for Test Devices No. 4 and No. 5, (i.e., symmetric ball devices, without and with a dielectric, respectively) indicate there was an average negative residual force at 19 kV of

$$-0.0125 \pm 0.0027 \mu N.$$

Further, for test devices No. 4 and No. 6 (i.e., the same symmetric ball device without a dielectric, and a symmetric plate device without a dielectric) there was an average negative residual force at 19 kV of

$$-0.0126 \pm 0.0029 \mu N.$$

These two values, and correspondingly close average values for each of the 15 kV and 10 kV conditions, show that the average residual forces for these symmetric device types was very small, was nearly independent of the actual type of symmetric device tested, and did not appreciably depend on the presence or absence of a dielectric. Further, these residual forces scale approximately with the square of the applied voltage over this 10 kV to 19 kV range.

Accordingly to Brown, [5] these symmetric devices should generate zero propulsive forces. The fact that they are not zero

Table 7. Residual Force Data Summary

		Residual Force - μN $\pm$ 1σ		
Device No.	**Device Configuration**	**19 kV**	**15 kV**	**10 kV**
4	Sym. Ball, No Diel.	-0.0108 $\pm$ 0.0004	-0.0067 $\pm$ 0.0002	-0.0035 $\pm$ 0.0001
5	Sym. Ball, with Diel.	-0.0142 $\pm$ 0.0023	-0.0081 $\pm$ 0.0006	-0.0045 $\pm$ 0.0007
1B	Ball & Plate, No Diel.	+0.0016	+0.0028	-0.0001
2B	Ball & Plate, with 1/4" Diel.	-0.0243 $\pm$ 0.0034	-0.0156 $\pm$ 0.0022	-0.0074 $\pm$ 0.0011
3	Ball & Plate, with 1/2" Diel.	+0.0021 $\pm$ 0.0021	-0.0004 $\pm$ 0.0019	-0.0015 $\pm$ 0.0011
4	Sym. Ball, No Diel.	-0.0108 $\pm$ 0.0004	-0.0067 $\pm$ 0.0002	-0.0035 $\pm$ 0.0001
6	Sym. Plate, No Diel.	-0.0143 $\pm$ 0.0025	-0.0094 $\pm$ 0.0018	-0.0042 $\pm$ 0.0011

Table 8. Force Amplitude Data Summary

		Force Amplitude - μN $\pm$ 1σ		
Device No.	**Device Configuration**	**19 kV**	**15 kV**	**10 kV**
4	Sym. Ball, No Diel.	0.1992 $\pm$ 0.0004	0.1241 $\pm$ 0.0002	0.0542 $\pm$ 0.0001
5	Sym. Ball, with Diel.	0.1638 $\pm$ 0.0023	0.1055 $\pm$ 0.0006	0.0478 $\pm$ 0.0007
1B	Ball & Plate, No Diel.	0.3316	0.2090	0.0905
2B	Ball & Plate, with 1/4" Diel.	0.3596 $\pm$ 0.0044	0.2256 $\pm$ 0.0029	0.0995 $\pm$ 0.0015
3	Ball & Plate, with 1/2" Diel.	0.2999 $\pm$ 0.0021	0.1880 $\pm$ 0.0019	0.0827 $\pm$ 0.0011
4	Sym. Ball, No Diel.	0.1992 $\pm$ 0.0004	0.1241 $\pm$ 0.0002	0.0542 $\pm$ 0.0001
6	Sym. Plate, No Diel.	0.2975 $\pm$ 0.0026	0.1840 $\pm$ 0.0019	0.0811 $\pm$ 0.0012

is of interest, since it suggests forces may have arisen from some other cause.

It will also be noted that the residual forces given in Table 7 for Test Devices No. 1B (without a dielectric), No. 2B (with a 1/4-in diameter dielectric) and No. 3 (with a 1/2-in diameter dielectric) showed erratic results. All the residual forces observed for Test Devices No. 1B and No. 3 were near or below the measurement threshold of $\pm$ 0.002 μN. As further indication that these values may only represent "noise," the sign (or direction) and magnitude of the force did not appear to vary with any particular functional relationship to the driving voltage.

The forces for device 2B were roughly twice the average values indicated previously for the symmetric devices, were in the same direction, and fell even further outside the measurement threshold limits than the forces observed for the symmetric devices. It does not seem possible without further consideration to reconcile the average residual force values observed for Test Device No. 2B, with those observed for Test Devices Nos, 1B and 3. This issue will be noted later in the section on Evaluation.

A final aspect of the device tests was concerned with the measurement of electric current through the test devices by means of the electrometers installed in the upper and lower conducting fibers. The approach used was an attempt to overcome the difficulties of measuring very small currents in the pico-ampere range, at voltage levels of tens of kV, remotely, in a vacuum chamber. This approach was useful, but was not nearly as successful as we had hoped.

The electrometers were used during approximately a third of the total tests, but measurements of device current were still

difficult to obtain. The electrometer units turned out to be quite sensitive to electrical "noise" within the chamber, even though inside the chamber they were each placed within a separate stainless steel enclosure, with one end covered with aluminum foil. Successful measurements of device current were made on very few of the tests conducted. A representative set of absolute values of the average current through each test device indicated by the electrometers is shown in Figure 18 for Test Nos. 41 and 42. The test devices in these runs were of type 2B--a ball and plate unit with a 0.00635 m (0.250 in) diameter acrylic rod between electrodes. The voltage polarity of the plate electrode in Test No. 41 was negative, and in Test No. 42 it was positive; the ball electrode in each case was at the same earth ground as the chamber wall. The direction of the current in Test No. 41 is from the ball toward the plate, as expected, and this direction is reversed in Test No. 42, since the power supply voltage was reversed.

Below ten kV,

Below ten kV, the average indicated current was about t pico amperes (pA) total, or one pA per test device. This corresponded to the approximate measurement threshold of the electrometer system.

The variation of average current, $\bar{i}$, through device 2B with applied potential difference, V, shown in Figure 18 can be represented by the simple functional form

$$\bar{I} = aV^b, \qquad (15)$$

above the measurement threshold. This regression line, when passed through the very limited number of points of Test Nos. 41 and 42 becomes

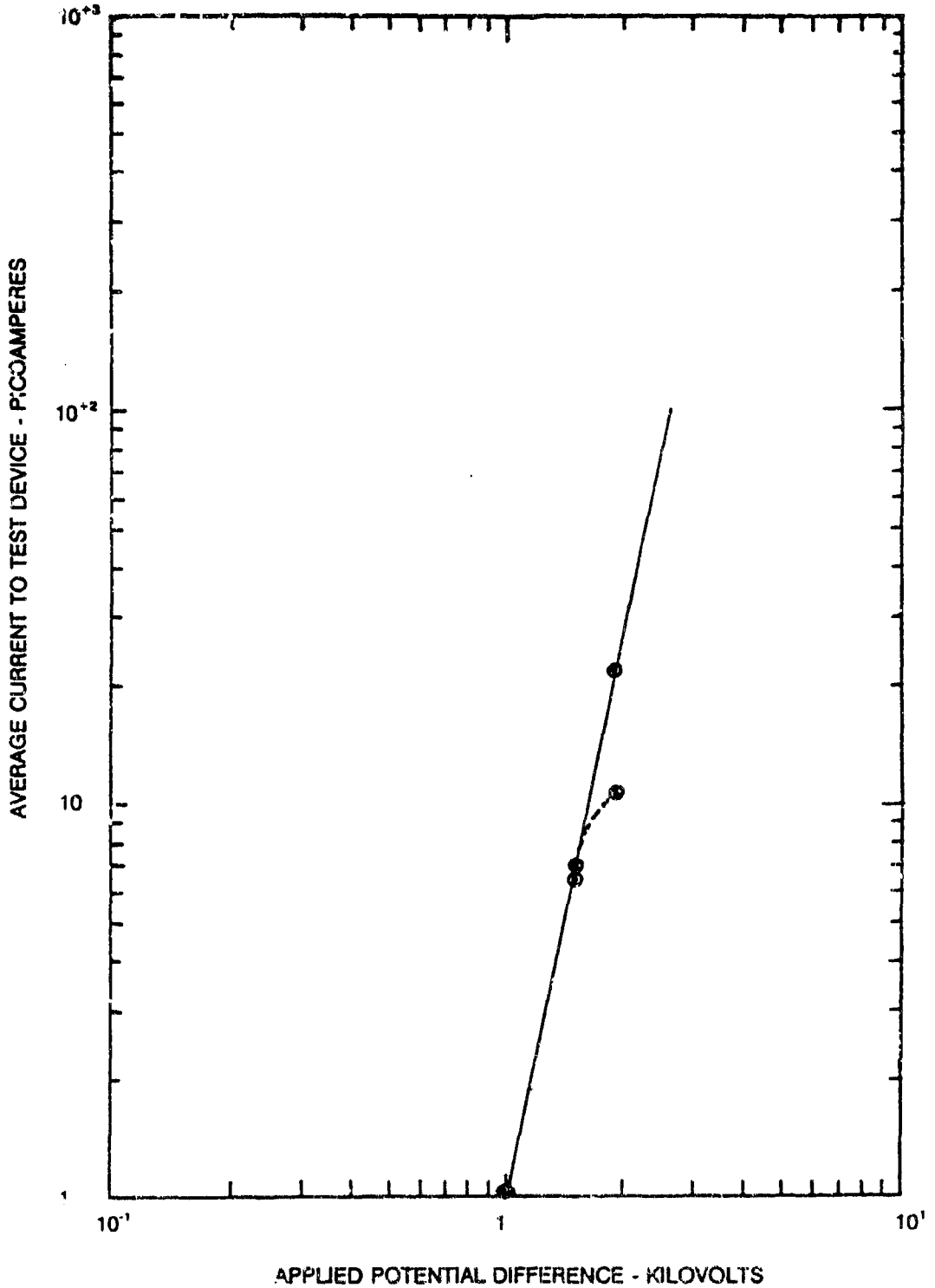

Figure 18. Variation of Average Current Through A Typical Test Device (No. 2B) With Applied Potential Difference

$$\bar{I} = 1.58 \times 10^{-5} V^{4.79}, \qquad (16)$$

where $\bar{I}$ is expressed in pico amperes (pA) and V is in kilovolts (kV). It will be observed that the value of current at 19 kV for Test No. 42 is not well represented by Expression (16), even though the currents at lower levels are.

The exponents in the preceding functional form are rather sensitive to the actual data, and hence, to minor systematic errors in the measured values. The values given, therefore, should be considered only as representative. Scant data from other tests suggest these absolute values may vary by perhaps a factor of two or so from the values calculated using Expression (16).

System Errors

Any measurement system is subject to errors, both random and systematic, and the torsion fiber system used in this effort was no exception.

The main random errors were associated with the actual---and in some cases only a suspected---zero shift of the equilibrium position of the torsion pendulum. This zero shift was not observed during the early boundary effects tests, but became apparent after Test No. 62. A problem was suspected with the force measurements during Test Nos. 50 and 53, but routine observations of the fiber tensioning mass at the bottom of the chamber showed no apparent motion or change in angular position of this mass with respect to the conducting platform on which it rested. Later, it become apparent that mechanical vibration, presumably induced by the backup mechanical vacuum pump, was causing the tensioning mass to shift its angular position

slightly after the mass was lowered onto the platform. This shift was not consistent, and apparently caused the fiber to twist sufficiently to alter the effective calibration value slightly. This problem was addressed during Tests Nos. 63 through 66 and was overcome by reducing the vibration level. The absence of such angular shifts was checked subsequently by noting the equilibrium positions of the pendulum before and after lowering the tensioning mass. As a result of this finding, selected tests of device Nos. 5 and 6 were repeated to confirm earlier findings.

The main systematic effects encountered were associated with electrostatically induced boundary forces which affected the behavior of test devices mounted on the torsion pendulum. Initially it was unknown if all of these effects could be accounted for, or if some would remain as systematic errors, or if Brown-type residual forces could be identified as part of the observed effects.

As noted earlier, considerable effort was expended to minimize the boundary effects, but it became apparent that even with the application of conductive shields placed inside the vacuum chamber an appreciable induced force was present. This force acted on both the symmetric and asymmetric types of test devices during test runs. Also, this force was found to depend on the angular position of the test devices about the chamber vertical axis (which is indicated, equivalently, by the angular position of the zero torsion equilibrium condition of the pendulum) as a near periodic function which could be represented mathematically by Equation (14), [i.e. $F=a+b \sin(\theta-\alpha)$].

A force contribution with a dependence of the form "$b \sin(\theta-\alpha)$" can arise from electrostatically induced charges on the walls of the chamber if the axis of the torsion fiber is

parallel to, but offset from, the axis of cylindrical symmetry for the chamber.

The prospect of the fiber axis not being coincident with the chamber axis was rather likely, and a separation distance between the axes up to perhaps 5 mm (0.2 in) was possible.***** It is believed that such an axial offset of the torsion fiber was responsible for the approximate variation of the force amplitude with the sine of the angular phase (θ-α) of the torsion fiber equilibrium position.

The parameter "a" in Equation (14), represents an offset component of the total observed force, from zero. A non-zero value of "a" implied, at first sight, the existence of a steady, residual force component (in addition to the variable component noted above), which acted in the same direction over the complete set of torsion equilibrium positions observed, for a given test device type. As noted earlier, this steady force component could presumably arise from a steady force of the Biefield-Brown type. However, it is believed that a conventional explanation for this apparent steady force component is more likely the correct one, and this apparent force--rather that a Biefield-Brown type of force--was responsible for the non-zero values of "a" that were determined from observations.

This argument applies specifically to the tests and test results in which symmetric test devices were used, such as test device Nos. 4, 5 and 6 indicated in Table 2, and to the corresponding test results given in Table 7.

***** The vacuum chamber used was not of precision construction and the centers of the available top and bottom access ports in which the fibers were mounted could have been slightly off the chamber axis. Direct measurements did not indicate such an offset, but accurate measures within the chamber were difficult, and measures on the outside of the chamber were precluded because of a surrounding (empty) water jacket.

Experimentally, the equilibrium positions of the torsion pendulum were observed only over a 180° angular range, rather than over 360° of a true angular period. The 180° angular range used was expected to represent the effective angular period, since the pendulum was configured with two test devices mounted in tandem and 180° apart. Indeed, this would be the case if there were complete symmetry in the construction of the device holder and test devices. However, if the two test devices were held at only slightly different distances from the torsion fiber axis, and if the fiber axis was simultaneously offset from and parallel to the chamber axis, as shown in Figure 19, then an asymmetry effect would occur as indicated in Figure 20.

The device support orientation direction in Figure 19 corresponds to an equilibrium position "0" of the torsion pendulum. The positions labelled 0 through 8 correspond to a sequence of positions toward which the device support orientation arrow would point if the pendulum equilibrium position were changed in equal steps over the complete angular period of 360°. This same angular position sequence is indicated in Figure 20b and along the curve in Figure 20a. In Figure 20a, the curve represents schematically the apparent force that would be measured using a torsion fiber and the two tandem mounted symmetric test devices, as in the tests conducted in this program.

It will be noted from Figure 20a that the apparent force can be viewed as if it exhibited symmetry about the zero force axis in two regions (of 180° each), labelled "symmetric #1" and "symmetric #2." As shown, the maximum force amplitudes in symmetric #1 region are larger than those in symmetric #2. The curves in each region are not identically simple sine curves, but if the maximum amplitude difference between the regions is small, the curves can be closely approximated by sine curves.

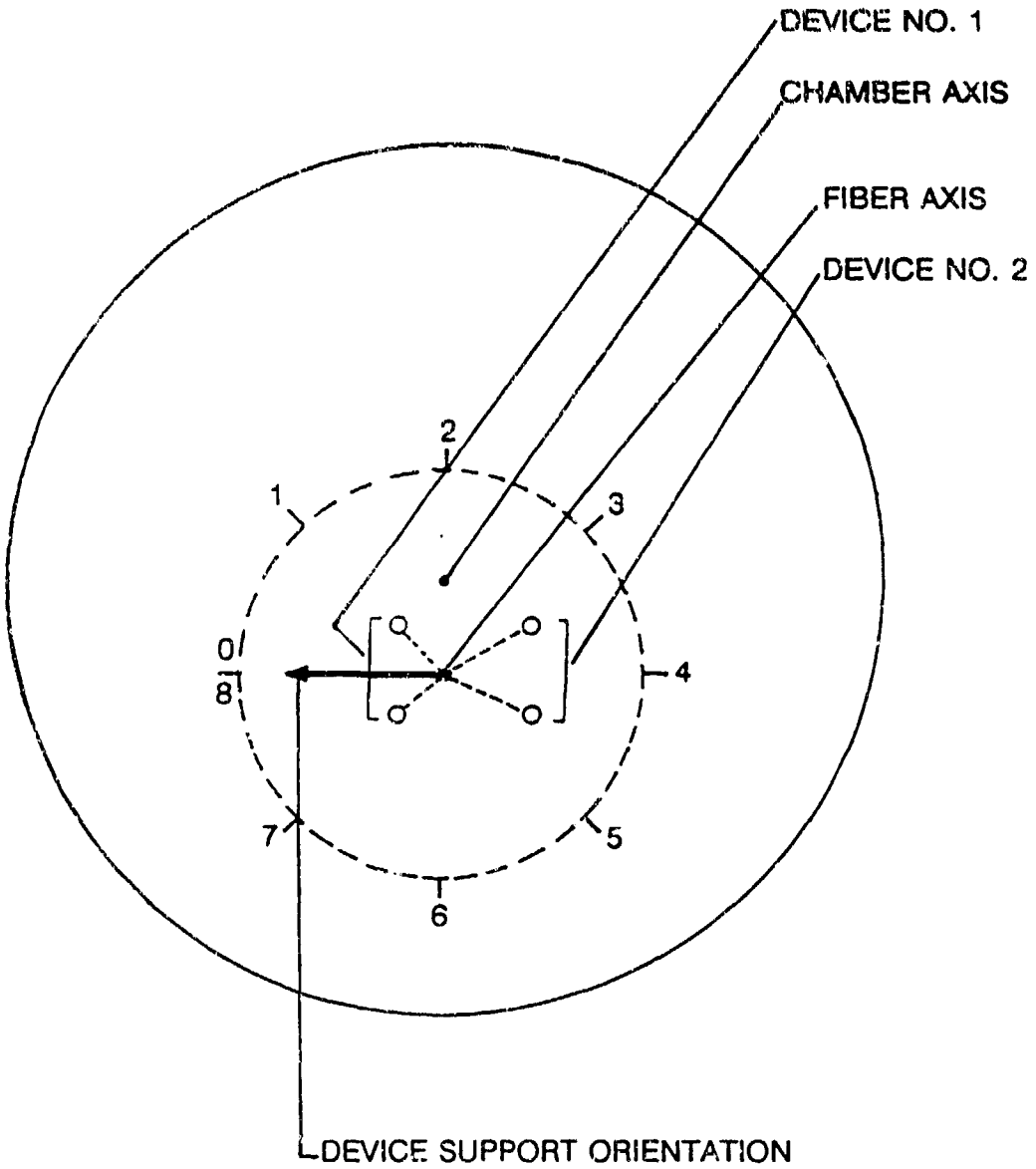

Figure 19. Orientations of Asymmetric Device Support Structure and Fiber Axis Offset

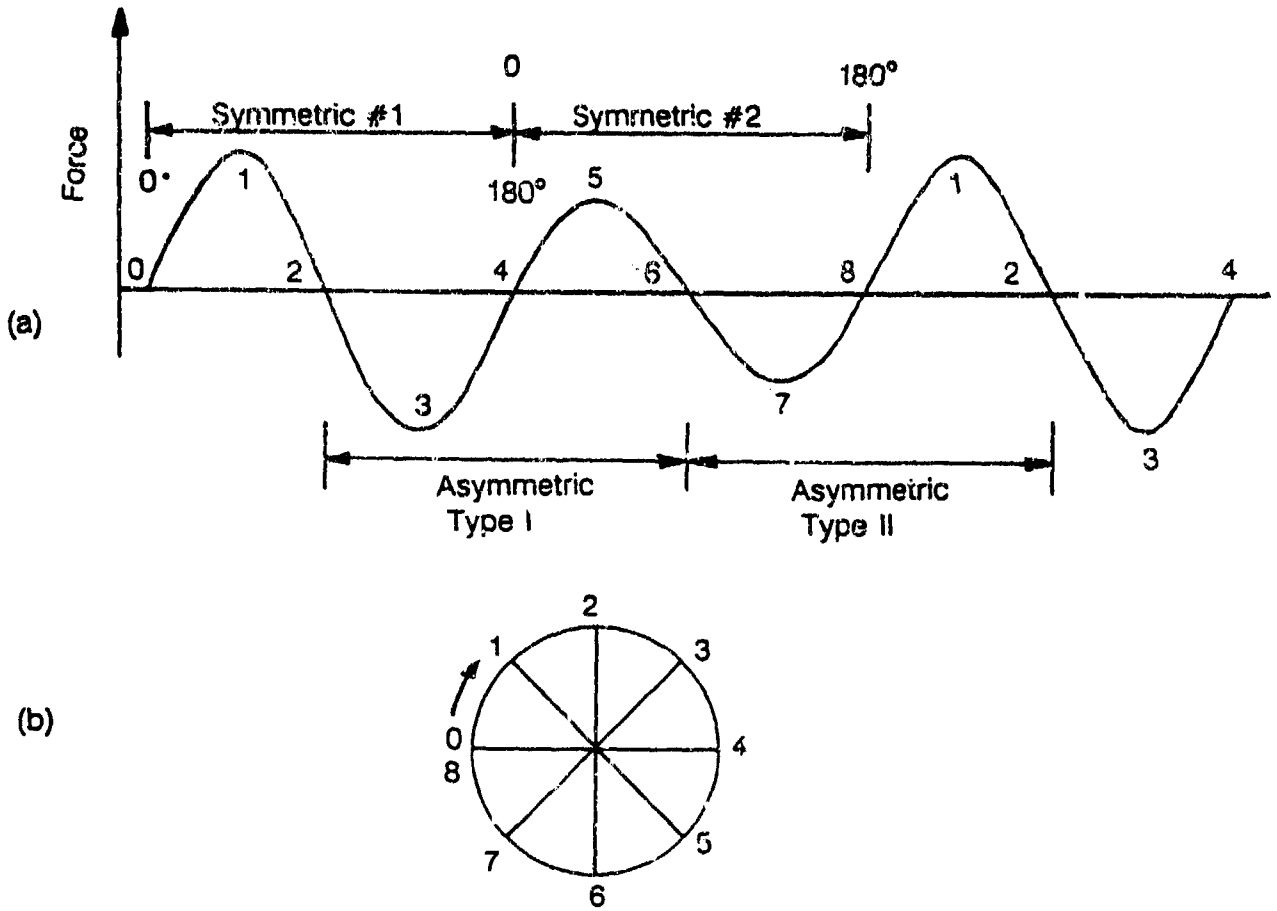

Figure 20. Asymmetry Effect from Device Support Structure and Offset Fiber Axis

Alternately, the apparent force in Figure 20a can also be viewed as if it exhibited asymmetry about the zero force axis in two other regions, designated "asymmetric type I" and "asymmetric type II." These regions are merely shifted 90° in angular phase of the torsion fiber equilibrium position, from the symmetric regions. Again these curves in each region are not identical simple sine curves, but can be closely approximated by sine curves, each with an apparent steady force component such as "a" in Equation (14).

If tests were conducted within the 180° region corresponding to "asymmetric type I," then negative values of "a" would be determined from force observations (as was found in this program). In the "asymmetric type II" region, positive values of "a" would be determined. In both of the symmetric regions the values of "a" would be essentially zero.

The prospect of the two test devices mounted on the support holder not being at the same distances from the fiber axis is certain. Care was taken to fabricate the small, 4.75 mm (0.187 in) diameter aluminum tubing support arms (shown in Figure 3 using a mechanical jig). Even so, when assembled, the moment arm to one device was 9.807 cm, and to the other was 9.750 cm, giving an average of 9.778 cm, and a difference of 0.057 cm (0.025 in). This difference amounts to only 0.58 percent of the average arm length. As such, it was not initially recognized as significant, and no attempt was made to reduce this moment arm difference. The average offset force determined for symmetric test devices Nos. 4 and 5 was -0.0125 μN (from Table 7); for the moment arm difference of 0.57 mm, this gives a value of 0.022 μN/mm. A similar result for the force amplitude of these same devices was 0.1845 μN (from Table 8), which for an assumed axial offset of 5.0 mm gives a value of 0.037 μN/mm. While these values are not identical, they are certainly of the same order, and tend to support the belief that the difference in

moment arm lengths of the test device support structure is the basis for the steady force component "a" observed in the symmetric device tests noted in Tables 6, 7 and 8.

Evaluation

The magnitudes of the total and residual force measurements need to be compared with estimates of the magnitudes of the electric wind and the ion propulsion effects to determine if the latter effects can account for any of the observed forces.

The total force measurements made under high vacuum conditions near 1.33×10^{-4} Pa (1.0×10^{-6} torr) were not expected to be influenced by electric wind effects, because the mean free path in N_2, or air, under these conditions is of the order of 50 m. This is many times the separation distance of the device electrodes, and, indeed, is also many times the largest linear dimension within the vacuum chamber used. The molecular density is simply not large enough to cause the entrainment of air molecules, and to cause electric wind effects under these conditions.

The magnitude of the ion propulsion effect depends on the size of the excess diffusion current emitted by one electrode over that collected by a second electrode within a test device. This excess or differential current was indicated by the electrometer in the propulsion device tests, was generally quite variable, and was not always consistent in sign or direction. Generally, these currents were well below about 100 pA (except during breakdown) during the tests run in a high vacuum. Thus, 1×10^{-10} A represents an approximate upper bound on the current expected to contribute to the ion propulsion effect in most of the tests.

A general expression for the force, F, expected from such an electrostatic thruster is given by Sutton and Ross[8]:

$$F = I\sqrt{\frac{2V\mu}{e}}, \qquad (17)$$

where

F= accelerating force, N
I= propelling current flow, A
V= accelerating potential difference, V
μ= mass of accelerated particle, kg
e= charge per particle, C.

For a threshold current of $I=10^{-10}$ A, V= 19 kV and $e= 1.60\times10^{-19}$ C, equation (17) gives

$$F = 48.7\sqrt{\mu}\ N.$$

If the accelerated particles were all electrons, protons, or aluminum ions (single charge), the corresponding maximum forces would be:

electrons: $\mu = 9.11 \times 10^{-31}$ kg
$F = 4.65 \times 10^{-14}$ N = 4.65×10^{-9} dyn

protons: $\mu = 1.672 \times 10^{-27}$ kg
$F = 1.99 \times 10^{-12}$ N = 1.99×10^{-7} dyn

aluminum ions: $\mu = 26.98 \times 10^{-27}$ kg/AMU = 44.8×10^{-27} kg
$F = 1.03 \times 10^{-11}$ N = 1.03×10^{-6} dyn.

The force per device would be one-half of each of these values.

These estimates assume that all the ion current would act collectively to propel each device in one direction. These force values per device are at most less than 1/400 of the force measurement threshold value of 2×10^{-9} N (0.0002 dyn).

Here, these estimates for ion propulsion effects are negligible.

This leaves a remaining question regarding reconciliation of the average residual force values observed and noted in Table 7 for Test Device No. 2B, with the values observed for Test Device Nos. 1B and 3.

In the previous discussion of systematic effects for symmetric test devices, it was argued that the observed residual forces in these tests were almost certainly artifacts associated with a combination of systematic errors. These errors included: an off-axis fiber; the construction asymmetry of the device holder; and the employment of an assumed 180° angular periodicity of pendulum equilibrium positions, rather than the complete 360° angular period. While only symmetric test devices were considered, it is expected that a similar effect would hold for asymmetric test devices, such as those used in Test Nos. 1B, 2B and 3. The residual force values determined for these tests with asymmetric devices, might not be exactly the same as those experienced with the symmetric devices. However, on the basis of the symmetric device tests with and without a dielectric, one would expect nearly identical force values to be observed for Test Devices Nos. 1B, 2B and 3. Since we became more aware of potential errors as the test program proceeded, and we paid greater attention to minimizing them, we now give greater credence to the residual force results obtained for Test Device Nos. 1B and 3, than for Test Device No. 2B. Full reconciliation cannot be given, but we tend to discount the residual force results obtained for Test Device No. 2B as being erroneous.

Anomalies

Near the end of this experimental program, we briefly examined the force generation effects with pulsed fields, which had a peak voltage of 19 kV. Test Nos. 56, 59, 62, 68 and 69 were conducted in this manner, using pulse repetition rates of 10, 60, 150, 400 and 600 Hz. Generally, no motion of the test devices was observed, except in Test No. 69 where a very small, but detectable motion was seen. For an input voltage of 19 kV during this test, the apparent force was about 0.007 μN (which is just above the force measurement threshold of 0.002 μN) and is not considered significant.

Two tests, Nos. 81 and 82 were conducted to examine the effect on forces generated by test devices where a dielectric was used which had a significantly larger dielectric constant than possessed by acrylic. Each of these two tests used test devices of type 2C with a ceramic piezoelectric material of lead titanate lead zirconate.****** This material had a dielectric constant of about 1750 along the length of the cylinder. The direction of dielectric poling was also along the length of the cylinder. The force generation results for both of these tests appeared anomalous.

A computer plot of the direct torsion pendulum positions for anomalous Test No. 81 is shown in Figure 21. The first set of deflections for the driving voltage steps of 5, 10, and 15 kV gave negative displacements, which appeared normal. When the voltage was increased to 19 kV, a slow pulsing breakdown was detected on the 0-2 mA meter mounted on the power supply. After one full swing of the pendulum, the voltage level was reduced

------

****** This material, designated channel 5500, was produced by Channel Products, Inc., 7100 Wilson Mills Road., Chesterland, Ohio 44026.

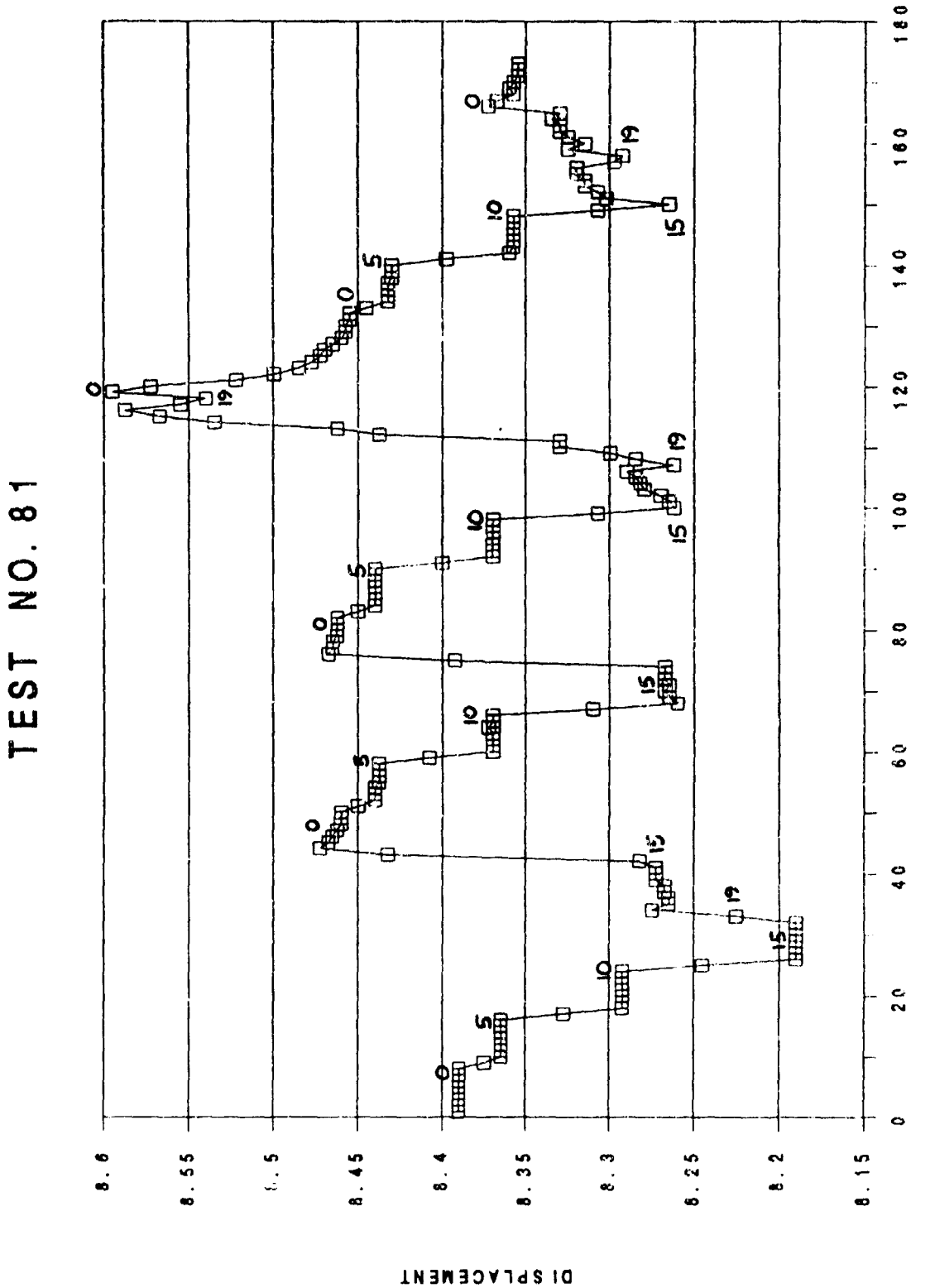

Figure 21. Torsion Pendulum Displacements For Anomalous Test No. 81

again to 15 kV. At 15 kV the displacements again stabilized, but had shifted from their original position before the breakdown pulse. The first set of voltage steps was completed by returning the voltage again to zero.

A second set of the same voltage steps was then started, and the pendulum displacements at 5, 10 and 15 kV were similar to those of the first set. There was an indication of minor pulsing breakdown at 15 kV for this set. This set was completed by returning the voltage to zero. This pendulum position at this new zero voltage setting was nearly the same as for the previous zero.

A third voltage set was then initiated, again using steps of 5, 10, and 15 kV. This time at 15 kV, more significant pulsing breakdown was experienced and the pendulum positions began to move toward larger numerical values (i.e., in the positive direction) while the pulsing continued. After a few oscillations of the torsion pendulum, the driving voltage was increased to 19 kV, and an even greater, slow pulsing breakdown occurred.

While this pulsing breakdown continued, the torsion pendulum began to move so the positions of its center of oscillation increased in value. Each point indicated in the position plots in Figure 21, represent the average pendulum position during one swing (one-half of a complete oscillation). The pendulum positions continued to change in the positive direction, opposite to the "normal" displacements from zero observed earlier for voltage steps of 5, 10 and 15 kV. These position changes continued to occur in the same direction for ten swings, or about 4.4 min, and then tended to reverse for two more swings (0.9 min) as if there had been an "overshoot" of position.

It is important to note that the observed rate of change of position in this case was rather slow, and it occurred with a

"constant" driving voltage applied to the test device (recognizing that the voltage may have fluctuated some during the breakdown pulses). This position change was not the same as a free release of the torsion pendulum, which might be expected to allow the pendulum to swing with increased amplitudes. The positions observed represent the positions of the centers of swing of the pendulum. Further, under normal conditions where breakdowns did not occur, the pendulum positions were usually almost constant for successive swings, and when the driving voltages were changed the positions typically responded to the new levels in one or two swings.

The driving voltage was then returned from 19 kV to zero. The pendulum position again increased for one swing in the positive direction. During the thirteen subsequent swings (5.7 min) the pendulum slowly returned to a "zero" position, very nearly the same as the zero position at the start of this voltage set.

A final voltage set was then run, and at 15 kV a pulsing breakdown again occurred; this was accompanied by a positive pendulum displacement as for the previous 15 kV voltage step. The voltage was then increased to 19 kV, large additional breakdowns occurred, and a small negative displacement jump was observed. This time, however, the large positive displacement shift observed previously was not repeated, and the final zero voltage step did not return the pendulum position to its value at the beginning of this last voltage set.

A complete plot of the torsion pendulum for Test No. 82 is shown in Figure 22. For this test, the first voltage step applied was 19 kV, to achieve pulsing voltage breakdowns within the test devices similar to those developed during Test No. 81.

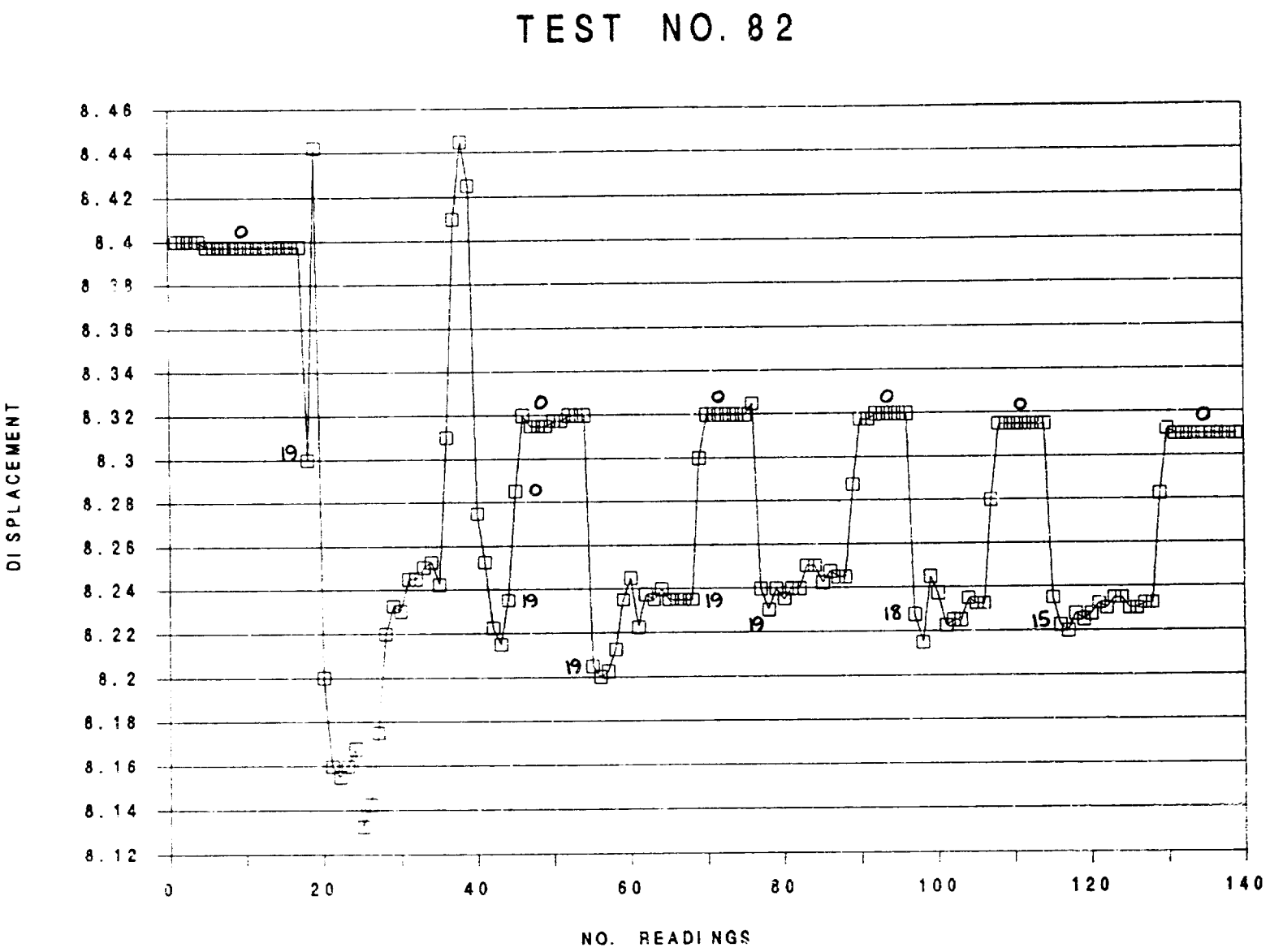

Figure 22. Torsion Pendulum Displacements For Anomalous Test No. 82

Such breakdowns did occur and the rate at which they pulsed was variable during the 11.7 min while the applied voltage was maintained (relatively) constant. Rather sizeable changes in pendulum position opposite to the "normal" direction were observed during this first 19 kV voltage step, similar (but less consistent) than those observed in Test No. 81.

Finally, the applied voltage was returned to zero, and the pendulum position assumed a new zero reading rather than the original reading.

Next, a second 19 kV voltage level was applied. In this case, the breakdown pulses were slow for the first two pendulum positions plotted. They then occurred faster and the pendulum position began moving toward larger values. After four such swings, the pulse rate again slowed for a swing, the pendulum position decreased and then finally stabilized after a few more swings.

The voltage was again returned to zero, and the pendulum position also returned to essentially the same zero as it was for the previous cycle.

A third voltage level of 19 kV was applied, and similar, but less pronounced pendulum position changes toward larger values were observed. The voltage was then returned to zero, and the pendulum position also returned to the same zero position.

A fourth voltage level of 18 kV was applied and the breakdown pulsing rate was fast at first, then slowed after the first four swings. The pendulum positions responded just as in the earlier 19 kV case where the pulsing rate was noted. When the voltage level was changed to zero, the pendulum position also returned to (near) the same position zero.

The final voltage level applied was 15 kV, and the associated pendulum position behavior was similar to that for the previous voltage step.

The force behaviors in Test Nos. 81 and 82 remain anomalous---compared with the results observed when no breakdowns were occurring across the dielectric in the test devices. From visual observations, it was noted that the electrical breakdowns were occurring in the vicinity of the dielectric. These were probably breakdowns over the surface of the dielectric rods, rather than through their interior, but this could not be distinguished by visual observations.

Key observations made during these tests can be summarized as follows:

- The anomalous force was associated with the occurrence of electrical breakdowns over (or through) the piezoelectric dielectric between electrodes held at a potential difference of about 19 kV.

- The anomalous force seemed to increase as the rate of breakdown pulsing increased, even though the observed pulsing rates were no more than a few pulses per second.

- The anomalous force acted in a direction opposite to the direction of the conventional electrostatically induced boundary force for these two tests (this may not be true in general). This suggests that the anomalous force is not due to electrostatic charges induced, generated, or somehow caused to appear on the test devices, since the boundary type forces arising from the presence of charge are independent of the sign of the charge.

- The piezoelectric nature of the dielectric material may be important to the anomalous force generation, as no similar results were observed during occasional electrical breakdowns when an acrylic dielectric was used between electrodes of the various devices tested.

- Rather significant current pulses were likely associated with the observed electrical breakdowns. The magnitudes of the current in the pulses are unknown, but they could be large, since meter readings on the power supply indicated current pulses up to about one mA.

- The anomalous force is not believed to be associated with some artifact of current pulses passing through and temporarily altering the properties or calibration of the torsion fiber force measuring system Small values of the anomalous force left the zero equilibrium positions of the torsion pendulum (at zero applied voltage) unaltered, once the anomalous force was removed. The return of the pendulum to its zero position seemed to be just as rapid, in most cases, whether a pendulum position shift was caused by a conventional electrostatic boundary force or the anomalous force.

CONCLUSIONS

The following conclusions have been reached based on the investigations of the Biefield-Brown effect conducted on this project:

1. Direct experimental results show that under high vacuum conditions, with air pressures in the approximate range of 1.33×10^{-3} Pa (1.0×10^{-5} torr) to 6.3×10^{-5} Pa (5.0×10^{-7} torr), no detectable propulsive force was electrostatically induced by applying a static potential difference up to 19 kV between test device electrodes, either with or without a spatial divergence of the electric field and energy density within that field. The minimum detectable force in these experiments was about 2×10^{-9} N.

2. The electrostatically generated propulsive force, which was claimed to exist by T.T. Brown for test devices driven by steady electrostatic potential differences between the device electrodes, under high vacuum conditions "when there was no vacuum spark," was not observed. If such a force still exists and lies below the threshold of measurements in this program, then the force may be too small to be attractive for many, if not most, space propulsion applications.

3. The boundary effects associated with making electrostatically induced propulsive force measurements, such as those explored under this program, are severe inside a vacuum chamber of small or moderate size with conducting walls (and presumably also with dielectric walls). Great care must be exercised in achieving adequate symmetry in the complete measurement configuration so that sufficiently small force levels can be detected and measured.

Experimental difficulties are exacerbated by the need to conduct tests remotely within a chamber under a high vacuum.

4. Steady electrostatic potential differences somewhat higher than 19 kV (up to 33 kV) were occasionally obtained during the tests, but there was no indication that any significant nonlinearities were induced in any of the test devices which would cause significant propulsive forces to develop using such techniques.

5. Anomalous propulsive force generation results were obtained during two tests with a ball and plate type of test device when these electrodes were separated by a high dielectric constant, ceramic piezoelectric material, and only when electrical breakdowns occurred between the electrodes. The magnitude of the anomalous force observed tended to increase as the rate of breakdown pulsing increased, even though the observed pulsing rates were no more than a few pulses per second.

RECOMMENDATIONS

As a result of this investigation, it is recommended that the investigation of propulsive forces generated on test devices by the action of abrupt electrical breakdown (and possibly other type) pulses applied to piezoelectric and/or select dielectric materials be continued. The purpose of this activity would be to further explore and verify the existence of the "anomalous force" noted in this report. Such investigations should initially be conducted without the complication of operating within a vacuum chamber. Verification of promising results in a vacuum environment will be necessary at the appropriate time. Further consideration needs to be given to techniques for measuring such anomalous forces directly, since torsion fiber based systems may not be appropriate.

It is also recommended that no further effort be expended on DC voltage driven propulsive force generation systems of the type examined under this program.

REFERENCES

1. R.L. Talley, 21st Century Propulsion Concept, AFAL-TR-88-031, April 1988, Final Report on AF Contract No. F04611-87-C-0058 with Veritay Technology, Inc., P.O. Box 305, East Amherst, NY 14051.

2. R.L. Talley, 21st Century Propulsion Concept. Final Report on NYS Contract No. SBIR (88)-166 of NYS Science and Technology Foundation with Veritay Technology, Inc., P.O. Box 305, East Amherst, NY 14051.

3. D.E. Gray (ed.), American Institute of Physics Handbook, McGraw-Hill Book Co., New York, 1957, pp.2-61, 3-78, 3-80.

4. A. Elliott and J.M. Dickson, Laboratory Instruments: Their Design and Application, Chemical Publishing Co., New York, 1960.

5. T.T. Brown, Electrokinetic Apparatus, U.S. Patent 3,187,206 June 1, 1965.

6. A.A. Andronov and C.E. Chaikin, Theory of Oscillations, Princeton Univ. Press, Princeton, 1949.

7. W.E. Deming, Statistical Adjustment of Data, Dover Publications, New York, 1964, (See especially Sections 20 and 62).

8. G.P. Sutton and D.M. Ross, Rocket Propulsion Elements, 4th ed., John Wiley and Sons, New York, 1976, p 481.